

Restricted diet delays accelerated ageing and genomic stress in DNA-repair-deficient mice

W. P. Vermeij^{1*}, M. E. T. Dollé^{2*}, E. Reiling^{1,2}, D. Jaarsma³, C. Payan-Gomez^{1,4}, C. R. Bombardieri¹, H. Wu⁵, A. J. M. Roks⁵, S. M. Botter^{1,6}, B. C. van der Eerden⁷, S. A. Youssef⁸, R. V. Kuiper^{8†}, B. Nagarajah², C. T. van Oostrom², R. M. C. Brandt¹, S. Barnhoorn¹, S. Imholz², J. L. A. Pennings², A. de Bruin^{8,9}, A. Gyenis¹, J. Pothof¹, J. Vijg¹⁰, H. van Steeg^{2,11} & J. H. J. Hoeijmakers^{1,12}

Mice deficient in the DNA excision-repair gene *Ercc1* (*Ercc1*^{Δ/−}) show numerous accelerated ageing features that limit their lifespan to 4–6 months^{1–4}. They also exhibit a ‘survival response’, which suppresses growth and enhances cellular maintenance. Such a response resembles the anti-ageing response induced by dietary restriction (also known as caloric restriction)^{1,5}. Here we report that a dietary restriction of 30% tripled the median and maximal remaining lifespans of these progeroid mice, strongly retarding numerous aspects of accelerated ageing. Mice undergoing dietary restriction retained 50% more neurons and maintained full motor function far beyond the lifespan of mice fed *ad libitum*. Other DNA-repair-deficient, progeroid *Xpg*^{−/−} (also known as *Ercc5*^{−/−}) mice, a model of Cockayne syndrome⁶, responded similarly. The dietary restriction response in *Ercc1*^{Δ/−} mice closely resembled the effects of dietary restriction in wild-type animals. Notably, liver tissue from *Ercc1*^{Δ/−} mice fed *ad libitum* showed preferential extinction of the expression of long genes, a phenomenon we also observed in several tissues ageing normally. This is consistent with the accumulation of stochastic, transcription-blocking lesions that affect long genes more than short ones. Dietary restriction largely prevented this declining transcriptional output and reduced the number of γH2AX DNA damage foci, indicating that dietary restriction preserves genome function by alleviating DNA damage. Our findings establish the *Ercc1*^{Δ/−} mouse as a powerful model organism for health-sustaining interventions, reveal potential for reducing endogenous DNA damage, facilitate a better understanding of the molecular mechanism of dietary restriction and suggest a role for counterintuitive dietary-restriction-like therapy for human progeroid genome instability syndromes and possibly neurodegeneration in general.

Dietary restriction is the best-documented intervention for extending lifespan in numerous species and retards many symptoms of ageing^{7–10}. Despite extensive research, its underlying mechanisms are still unresolved, although suppression of growth hormone/insulin-like growth factor 1 (GH/IGF1) and mechanistic target of rapamycin (mTOR) signalling are likely implicated^{8,10}. The molecular underpinnings of ageing itself are also poorly understood, although the fact that progeroid syndromes are associated with impaired genome maintenance⁴ points towards a connection with compromised genome stability^{11,12}. Links between the accumulation of DNA damage and the GH/IGF1 axis emerged when DNA-repair-deficient progeroid

mice were found to have a suppressed GH/IGF1 somatotrophic axis and upregulated anti-oxidant defences, presumably in an attempt to extend their lifespan by redirecting resources from growth to cellular maintenance and stress resistance^{1,5}. Normal mice and mammalian cells also share this ‘survival response’ after the induction of persisting DNA damage, indicating that it is a common response^{1,5,13}.

Growth-suppressed progeroid DNA-repair mutants show spontaneous dietary-restriction-like responses alongside other signs suggestive of dietary restriction, including reduced subcutaneous fat and paradoxical features of delayed ageing^{14,15}. We therefore wondered whether subjecting progeroid mice to actual dietary restriction would be beneficial or, in view of their poor growth and frail appearance, detrimental. We subjected *Ercc1*^{Δ/−} progeroid DNA-repair mutants, with a lifespan of only 4–6 months^{3,16,17}, to gradual food restriction. Mice initially had food restricted by 10% at week 7, with restriction reaching a maximum of 30% from 9 weeks onwards. Dietary restriction in both genders extended median and maximal remaining lifespan by approximately 200%; the median lifespan of males increased from 10 to 35 weeks (250% extension; $P < 0.0001$) and that of females increased from 13 to 39 weeks (200% extension; $P < 0.0001$) (Fig. 1a, b).

As lifespan can be influenced by factors other than food¹⁸, we repeated the study in another animal facility with different housing but similar food and a similarly restricted diet. A dietary restriction of 30% extended median remaining lifespan by 180% ($P < 0.0001$; Fig. 1c). We decided to test another repair-deficient progeroid mutant, the Cockayne syndrome-like *Xpg*^{−/−} mouse. This genotype carries defects in partially different DNA repair pathways² and has an even shorter lifespan than the *Ercc1*^{Δ/−} mutant (approximately 18 weeks versus 22–25 weeks)⁶. The same dietary restriction regimen induced a significant increase in remaining median lifespan of approximately 80% ($P < 0.0001$, Fig. 1d), widening the scope of dietary restriction beyond *Ercc1* mutants. Even a six-week dietary restriction interval, from 6 to 12 weeks of age, yielded a striking median lifespan extension of 6 weeks for *Ercc1*^{Δ/−} mice ($P = 0.0042$) and 4 weeks for *Xpg*^{−/−} mice ($P < 0.0001$; Fig. 1c, d), indicating that the effect brought about by dietary restriction persists, consistent with reducing the short-term death risk found in *Drosophila*¹⁹. When comparing *Ercc1*^{Δ/−} with *Xpg*^{−/−} it should be noted that *Xpg*^{−/−} animals were already biologically older when dietary restriction started. Although *Ercc1*^{Δ/−} and *Xpg*^{−/−} mice fed *ad libitum* never become obese, upon dietary restriction, their bodyweights uniformly stabilized to gender- and genotype-specific

¹Department of Molecular Genetics, Erasmus University Medical Center Rotterdam, PO Box 2040, 3000 CA Rotterdam, The Netherlands. ²Centre for Health Protection, National Institute for Public Health and the Environment (RIVM), PO Box 1, 3720 BA Bilthoven, The Netherlands. ³Department of Neuroscience, Erasmus University Medical Center Rotterdam, PO Box 2040, 3000 CA Rotterdam, The Netherlands. ⁴Facultad de Ciencias Naturales y Matemáticas, Universidad del Rosario, Carrera 24, 63C-69 Bogotá, Colombia. ⁵Department of Internal Medicine, Division of Vascular Medicine and Pharmacology, Erasmus University Medical Center Rotterdam, PO Box 2040, 3000 CA Rotterdam, The Netherlands. ⁶Laboratory for Orthopedic Research, Balgrist University Hospital, Forchstrasse 340, 8008, Zürich, Switzerland. ⁷Department of Internal Medicine, Erasmus University Medical Center Rotterdam, PO Box 2040, 3000 CA Rotterdam, The Netherlands. ⁸Dutch Molecular Pathology Center, Department of Pathobiology, Faculty of Veterinary Medicine, Utrecht University, PO Box 80125, 3508 TC Utrecht, The Netherlands. ⁹Department of Pediatrics, Division Molecular Genetics, University Medical Center Groningen, PO Box 30001, 9700 RB Groningen, The Netherlands. ¹⁰Department of Genetics, Albert Einstein College of Medicine, 1300 Morris Park Avenue, Bronx, New York 10461, USA. ¹¹Department of Human Genetics, Leiden University Medical Center, PO Box 9600, 2300 RC Leiden, The Netherlands. ¹²CECAD Forschungszentrum, Universität zu Köln, Joseph-Stelzmann-Straße 26, 50931 Köln, Germany. †Present address: Department of Laboratory Medicine, Karolinska Institute, SE-171, 77 Stockholm, Sweden.

*These authors contributed equally to this work.

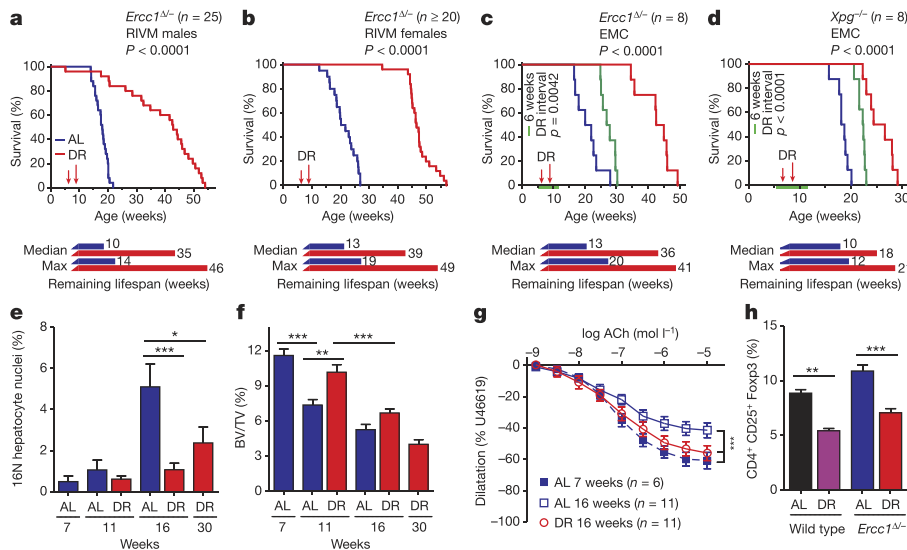


Figure 1 | Dietary restriction extends health and lifespan of *Ercc1*^{Δ/Δ} and *Xpg*^{-/-} mouse mutants. **a–d**, Survival of mice with *ad libitum* access to AIN93G diet or on 30% dietary restriction (dietary restriction, red; *ad libitum*, blue throughout) at two separate test sites. Male (**a**) and female (**b**) *Ercc1*^{Δ/Δ} mice, group housed at the National Institute for Public Health and the Environment (RIVM) ($n = 20–25$ animals per group, separate experiments), and *Ercc1*^{Δ/Δ} (**c**) and *Xpg*^{-/-} (**d**) mice, solitary housed at the Erasmus University Medical Center Rotterdam (EMC) ($n = 8$ animals per group, 4 of each gender), under *ad libitum* or dietary restriction regimens. Dietary restriction was initiated at 7 weeks of age with 10% restriction, and increased weekly by 10%, until 30% was reached from 9 weeks onward. Remaining median and maximum lifespan are indicated (week 8 was considered the start of effective dietary restriction). Simultaneously, a cohort of *Ercc1*^{Δ/Δ} (**c**) and *Xpg*^{-/-} (**d**) mice underwent temporary dietary restriction for 6 weeks (30% dietary restriction from 6 to 12 weeks)

(green; $n = 8$ animals per group, 4 of each gender). *P* values were calculated by the log-rank test. **e**, Quantification of 16N nuclei in hepatocytes of *ad libitum* or dietary restriction male *Ercc1*^{Δ/Δ} mice by FACS analyses; $n = 5$ animals per group. **f**, Trabecular bone volume fraction (bone volume/tissue volume) in femurs of *Ercc1*^{Δ/Δ} male mice, measured using micro-CT. *Ad libitum*- and dietary restriction-treated animals were analysed at different ages with $n \geq 6$ animals per group. **g**, Age-dependent decline of vasodilatation in *Ercc1*^{Δ/Δ} aorta segments, *ex vivo*. Dietary restriction-*Ercc1*^{Δ/Δ} aorta segments show significantly more relaxation at age of 16 weeks than *ad libitum*-*Ercc1*^{Δ/Δ} aorta. ACh, acetylcholine. **h**, Frequency of CD4⁺ CD25⁺ Foxp3⁺ T-regulatory cells among all CD4⁺ T cells from spleen of 16-week-old *Ercc1*^{Δ/Δ} mice under dietary restriction or *ad libitum* and aged-matched wild-type controls. $n \geq 3$ animals per group. Error bars denote mean \pm s.e. * $P < 0.05$, ** $P < 0.01$, *** $P < 0.001$.

values, persisting until the end of their extended lifespan. Paradoxically, however, when bodyweights of mice fed *ad libitum* approached the weight of diet-restricted mice, they died (Extended Data Fig. 1a–d).

As the extension of lifespan can be unrelated to ageing¹⁸, we examined key ageing parameters. *Ercc1*^{Δ/Δ} mutants exhibit exceptionally wide multi-morbidity, consistent with the notion that this protein is implicated in multiple DNA repair processes, including both transcription-coupled and global-genome nucleotide excision repair (NER) and crosslink repair². Ageing in *Ercc1*^{Δ/Δ} mice involves proliferative and post-mitotic organs, including the nervous system, liver, kidney, bone marrow, retina, muscle and the cardiovascular, skeletal, and gonadal systems^{1–4}. Additionally, they exhibit progressively declining vision and hearing, sarcopenia, cachexia, overall frailty and a variety of other features of ageing, many of which are also noted in XpF/Ercc1 (XFE) and other related human syndromes^{1,20,21}. Multisystem cross-sectional analyses showed that dietary restriction strongly attenuated virtually all features of premature ageing that were investigated, including anisokaryosis in the liver and kidney, formation of polyploid liver nuclei, kidney tubulonephrosis, osteoporosis, vascular dilatation, B- and T-cell immune parameters and testicular degeneration (Fig. 1e–h, Extended Data Figs 1–3 and Supplementary Table 1). Although the premature-ageing phenotype displays extreme multi-morbidity, an important cause of death of *Ercc1*^{Δ/Δ} mice is the progressive neurodegeneration that parallels NER-deficient premature ageing conditions in humans^{22,23}. Considering this translational relevance, we analysed neurological function in more detail. Longitudinal examination of behavioural abnormalities showed that the onset of tremors, imbalance, and paresis were greatly postponed or even absent in *Ercc1*^{Δ/Δ} and *Xpg*^{-/-} mice that underwent continuous or temporary dietary restriction regimes (Fig. 2a–c, Extended Data Fig. 4 and Supplementary Video 1). Dietary restriction strongly

improved motor function in *Ercc1*^{Δ/Δ} mice; at 16 weeks of age mice fed *ad libitum* displayed severe locomotor problems and frequently fell, whereas diet-restricted mice were fully capable of running (Fig. 2d and Supplementary Video 2). Even at ages far beyond the lifespan of mice fed *ad libitum*, locomotor function is well preserved in mice undergoing dietary restriction (Fig. 2e). In line with behavioural data indicating that neurological decline was virtually stopped, neurodegenerative pathology was strongly diminished by dietary restriction (including retinal photoreceptor loss, Golgi abnormalities, axonal swellings, astrocytosis and microgliosis) (Extended Data Figs 2e, 5, 6a, b). Notably, stereological counting revealed that diet-restricted animals retained approximately 50% more neurons in the neocortex than controls fed *ad libitum* (Fig. 2f), while the number of non-neuronal cells was similar (Extended Data Fig. 6c). Likewise, significantly more motor neurons were preserved in the spinal cord upon dietary restriction (Fig. 2g). These findings indicate that dietary restriction greatly improves health and lifespan in both *Ercc1* and *Xpg* repair-deficient mice and in particular attenuates neurodegeneration.

To examine whether the effects of dietary restriction in *Ercc1*^{Δ/Δ} mice resemble those in wild-type mice, we compared full-genome liver mRNA expression profiles in 11-week-old mice. Unbiased principal-component analysis of four groups: wild-type *ad libitum* (AL^{WT}), *Ercc1*^{Δ/Δ} *ad libitum* (AL^{Ercc1}), wild-type with 30% dietary restriction (DR^{WT}) and *Ercc1*^{Δ/Δ} with 30% dietary restriction (DR^{Ercc1}) revealed clear uniformity within and distinction between them, primarily based on dietary restriction and genotype (Fig. 3a). Of the 1,106 differentially expressed genes (DEGs) seen in DR^{Ercc1} mice, around two-thirds were also seen in DR^{WT} mice. Pertinently, expression levels of 684 out of the 688 common DEGs are also changed in the same direction in DR^{WT} and DR^{Ercc1} mice (Table 1 and Extended Data Table 1), indicating strong mechanistic parallels between both dietary restriction responses,

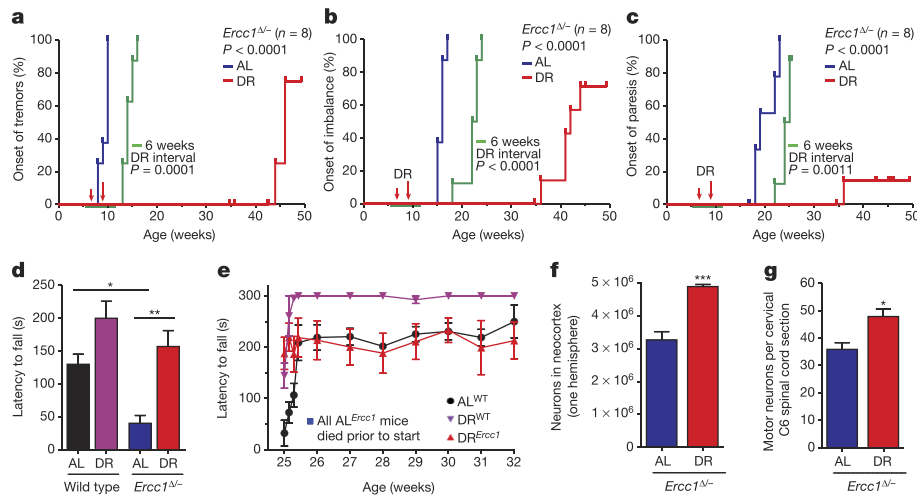


Figure 2 | Dietary restriction preserves neurological function.

a–c, Onset of neurological abnormalities (tremors **(a)**, imbalance **(b)**, paresis of the hind limbs **(c)**) with age in *ad libitum* and dietary restriction *Ercc1*^{Δ/Δ} mice. *n* = 8 animals per group. The onset of continuous dietary restriction is indicated by red arrows and the 6-week dietary restriction interval as green horizontal line. **d, e**, Average time spent on an accelerating rotarod of wild-type and *Ercc1*^{Δ/Δ} mice on different diets at 16 weeks of age (**d**; *n* = 8 animals per group) or weekly monitored beyond the lifespan of AL *Ercc1* mice (**e**; *Ercc1*^{Δ/Δ} *n* = 4, wild-type *n* = 3). A daily

training period was given at 25 weeks of age. **f, g**, Quantitative stereological analysis of the total number of neurons (**f**, NeuN⁺; *P* = 0.0008) in the neocortex of transverse brain sections and motor neurons (**g**, ChAT⁺; *P* = 0.0176) in C6 cervical spinal cord sections of 16-week-old *ad libitum* and diet-restricted *Ercc1*^{Δ/Δ} mice. Note that the selective effect on neurons is consistent with earlier observations that neurons are the primary target of *Ercc1* deficiency²⁸. *N* ≥ 3 animals per group. Error bars indicate mean ± s.e. **P* < 0.05, ***P* < 0.01, ****P* < 0.001.

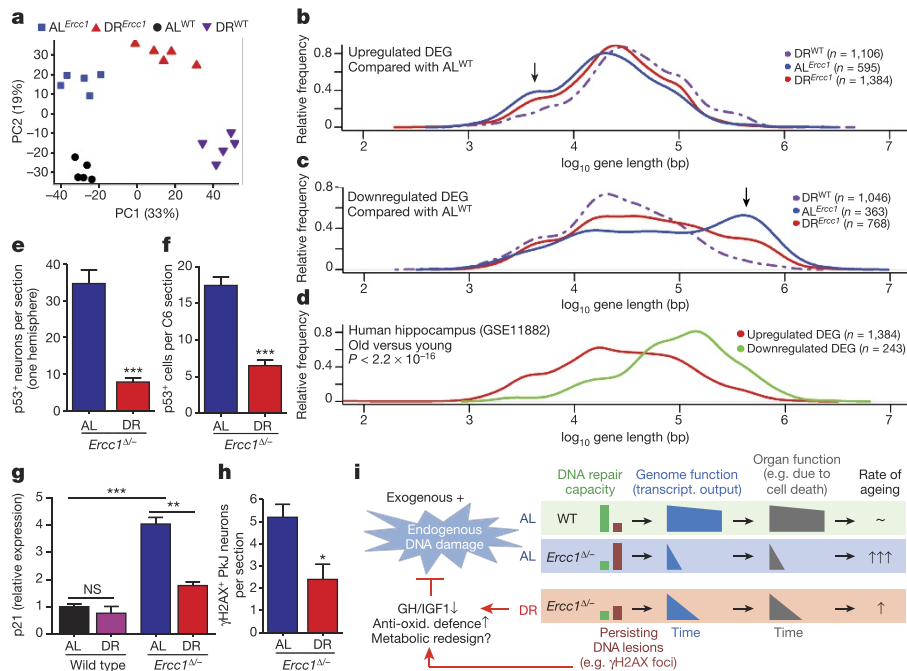


Figure 3 | Dietary restriction preserves genome function. **a**, Principal component analysis (PCA) of full genome liver RNA expression profiles of 11-week old AL *Ercc1* mice (blue squares), DR *Ercc1* (red triangles), AL^{WT} (black circles) and DR^{WT} (purple triangles) mice. This analysis takes into account all the genes in the microarray platform. The two main principal components, PC1 and PC2, explain 52% of the variability in the original data set: PC1 (*x* axis, 33%) differentiates on the basis of expression changes induced by dietary restriction, independent of genotype; PC2 (*y* axis, 19%) reflects differences associated with genotype. **b, c**, Relative frequency plot of gene length (log scale) of DEGs in DR^{WT} versus AL^{WT} (purple dashed lines), AL *Ercc1* versus AL^{WT} (blue lines) and DR *Ercc1* versus AL^{WT} (red lines). **b**, Only upregulated genes. **c**, Only downregulated genes. Black arrows, extra peak of upregulated short genes (**b**) and peak of downregulated long genes (**c**) in AL *Ercc1* mice. **d**, Relative frequency plot of gene length of DEGs in hippocampus from ~80-year-old humans versus ~20-year-old humans. Red, upregulated genes; green, downregulated genes. The DEGs

from human hippocampus were selected using a log₂-fold change cut-off of 0.5 and FDR < 0.05. The data set used corresponds to NCBI gene expression omnibus, number GSE11882. **e, f**, p53-positive cells counted in the neocortex of three consecutive transverse brain sections (**e**) at the level of the bregma (Mouse Brain Atlas, Paxinos) and three consecutive C6 cervical spinal cord sections (**f**). Sections from 16-week-old DR *Ercc1* mice (*n* = 4) show significantly reduced levels of p53-positive cells (*P* < 0.0001 for neocortex and *P* = 0.0002 for spinal cord) than sections from AL *Ercc1* mice (*n* = 4). **g**, Relative expression changes in the p53 target gene *p21* in 11-week-old wild-type and *Ercc1*^{Δ/Δ} mice induced by dietary restriction (*n* = 5). **h**, γH2AX-positive Purkinje (PkU) neurons were counted in cerebellum of five consecutive transverse brain sections from AL *Ercc1* and DR *Ercc1* mice (*P* = 0.014). Error bars indicate mean ± s.e. **P* < 0.05, ***P* < 0.01, ****P* < 0.001. **i**, Mechanistic model for the anti-ageing effect of dietary restriction.

Table 1 | Number of DEGs under dietary restriction

Comparison	DEG	Up	Down	Ratio	
				up:down	Concordant
DR ^{WT} vs. AL ^{WT}	2,704	1,522	1,182	1.29*	
DR ^{Ercc1} vs. AL ^{Ercc1}	1,106	669	437	1.53*	
Common	688	391	293		684
Enrichment factor	10.3	17.3	25.6		4

The number of differentially expressed gene (DEG) probes are shown for wild-type (WT) and *Ercc1*^{Δ/Δ} liver under dietary restricted (DR) and *ad libitum* (AL) conditions. **P* = 0.019 (Chi-square test with Yates correction).

consistent with overlapping Gene Ontology pathways and transcription factors (Supplementary Table 2). Molecular analyses of insulin, mTOR and GH/IGF1 signalling pathways and microRNA expression, amongst others, further support the parallels between DR^{WT} and DR^{Ercc1} gene expression (for example, the *GHR* gene, already suppressed in AL^{Ercc1} mice is further reduced upon dietary restriction; Extended Data Figs 1f, 7, 8a–e). These data revealed also an unexpected link between *Ercc1*-related DNA-repair deficiency and the unfolded-protein response (Extended Data Table 1 and Supplementary Table 2).

Transcription-coupled repair (TCR) deficiencies, which prevent resumption of RNA synthesis after transcription-blocking DNA damage in *Ercc1*^{Δ/Δ} mice, other mouse mutants and human patients, appear to be uniformly associated with premature ageing, affecting non- or slow-proliferating organs such as the nervous system, liver and kidney in particular². This suggests that time-dependent accumulation of transcription-blocking lesions contribute to accelerated ageing. Since DNA damage occurs stochastically, long genes generally accumulate more lesions and consequently become more transcriptionally crippled than short genes. Indeed, the DEGs of AL^{Ercc1} liver gene expression profiles at 11 weeks displayed a highly significant bias for long genes to be overrepresented in the class of downregulated genes and underrepresented in the category of upregulated genes (Fig. 3b, c, arrows). These and other data (Table 1 and Extended Data Table 2) suggest genome-wide accumulation of transcription-stalling lesions. We observed a similar, albeit milder, expression bias upon normal ageing in rat liver and human hippocampus (Fig. 3d and Extended Data Fig. 8f). Notably, dietary restriction in *Ercc1*^{Δ/Δ} mice strongly retarded this expression shift (red curve in Fig. 3b, c, and Extended Data Table 2).

That there were reduced DNA damage loads in DR^{Ercc1} mice is supported by an observed reduction in p53-expressing cells in the brain (Fig. 3e, f and Extended Data Fig. 6d), diminished apoptosis of retinal photoreceptors (Extended Data Fig. 6a) and preservation of neurons (Fig. 2f, g). We also found evidence for the suppression of p53 transcriptional activity in the liver of DR^{Ercc1} mice (Supplementary Table 2), further supported by dietary restriction-induced downregulation of expression of the microRNA miR-34a, a target of p53 (Extended Data Fig. 8c). Additionally, key senescence parameters, which were elevated in AL^{Ercc1} mice, were mitigated by dietary restriction. These include *p21* (also known as *Cdkn1a*) (Fig. 3g), *p16* (*Cdkn2a*) and *Il6* (Extended Data Fig. 8e). The proportion of Purkinje cell nuclei containing γH2AX foci, which reflect DNA breaks, appeared significantly reduced (Fig. 3h and Extended Data Fig. 6e). We conclude that dietary restriction concomitantly delays ageing, attenuates accumulation of genome-wide DNA damage and preserves transcriptional output, in all probability contributing to improved cell viability in *Ercc1* mutants (Figs 2f, g and 3c, h).

It seems unlikely that dietary restriction can overcome defects in DNA repair. It may be that dietary restriction reduces the induction and/or alters responses to damage, to which DNA repair mutants may over-respond. Indeed, the expression profiles of diet-restricted mice (Extended Data Figs 7, 8 and Supplementary Table 2) suggest that dietary restriction increases resistance to DNA damage-induced stress, improves antioxidant defences, alters insulin and other hormonal signalling pathways (redesigning major metabolic routes such

as glycolysis, oxidative phosphorylation and the pentose phosphate pathway), alters mitochondrial function and apoptotic responses and induces a shift from pro- to anti-inflammatory cytokines^{10,24}. Figure 3i presents a model that integrates our findings on dietary restriction, DNA damage and (accelerated) ageing. DNA damage from exogenous and endogenous sources accumulates with ageing and is accelerated in repair-deficient *Ercc1*^{Δ/Δ} mice. Stochastic DNA lesions reduce transcriptional output in a gene-size-dependent manner leading to cell dysfunction and death, stem cell exhaustion, organ and tissue atrophy and functional decline, which together cause ageing-related diseases. Both accumulation of DNA damage and dietary restriction trigger an anti-ageing response, which involves suppression of growth, upregulation of anti-oxidant defences and, presumably, metabolic redesign. This response reduces steady-state levels of reactive metabolites, thereby preserving genome integrity and delaying ageing-related functional decline.

Post-mitotic neurons have to reconcile one of the highest metabolic rates of the body with the preservation of a delicate homeostatic balance for over a century in humans. While everything else in cells can be turned over, the up-to-10⁵ daily DNA lesions per cell^{25,26} can only be repaired, requiring continuous efficient repair. That TCR defects are linked with severe neurodegeneration in Cockayne syndrome and trichothiodystrophy (TTD) indicates that removing transcription-obstructing lesions from the genome is vital for neuronal survival²³. Using tissue-specific repair mutants, we have shown that neurodegeneration is at least partly cell-autonomous^{6,27,28}, consistent with endogenous DNA damage being a main driver. The strong protection given by dietary restriction indicates that neurons possess considerable reserves to restrict DNA damage and prevent cell death. Cell-intrinsic mechanisms and systemic inflammatory and hormonal responses modulated by dietary restriction may contribute to the remarkable resilience of the neuronal system; they protect 50% more neurons from death, postpone the onset of tremors, imbalance and paresis and fully preserve motor performance (Fig. 2 and Supplementary Videos 1, 2). The notable preservation of neuronal function by dietary restriction in the *Ercc1*^{Δ/Δ} mutant is consistent with increasing evidence for the beneficial effects of dietary restriction in animal models of various neurodegenerative disorders^{29,30} and opens the door to nutritional and pharmacological interventions that could prevent the onset of these devastating diseases.

The strong evolutionary conservation of the dietary-restriction response, and the notable parallels between mouse and human symptoms, mean it is likely that the effect of dietary restriction is preserved from mouse to man. Therefore, an obvious future application may be the counterintuitive use of dietary restriction or pharmaceutical mimetics to treat DNA-repair-defective progeroid syndromes. Besides Cockayne syndrome and TTD, this may apply to xeroderma pigmentosum, combined xeroderma pigmentosum/Cockayne syndrome, cerebro-oculo-facio-skeletal (COFS) syndrome, Fanconi's anaemia, the RecQ-helicase-dysfunction driven family of conditions (Werner, Bloom's and Rothmund Thomson syndrome), ataxia telangiectasia, and others. Additionally, repair-deficient mice could prove to be useful tools for understanding anti-ageing interventions and helping to find alternatives to dietary restriction by strongly reducing the labour, time, costs and number of animals required, and also for defining the long-term health effects of nutrition.

Online Content Methods, along with any additional Extended Data display items and Source Data, are available in the online version of the paper; references unique to these sections appear only in the online paper.

Received 11 June 2015; accepted 25 July 2016.

Published online 24 August 2016.

- Niedernhofer, L. J. *et al.* A new progeroid syndrome reveals that genotoxic stress suppresses the somatotroph axis. *Nature* **444**, 1038–1043 (2006).
- Marteijn, J. A., Lans, H., Vermeulen, W. & Hoeijmakers, J. H. Understanding nucleotide excision repair and its roles in cancer and ageing. *Nat. Rev. Mol. Cell Biol.* **15**, 465–481 (2014).

3. Dollé, M. E. *et al.* Broad segmental progeroid changes in short-lived *Ercc1(-/Δ7)* mice. *Pathobiol. Aging Age Relat. Dis.* **1**, 10.3402/pba.v1i0.7219 (2011).
4. Vermeij, W. P., Hoeijmakers, J. H. & Pothof, J. Genome integrity in aging: human syndromes, mouse models, and therapeutic options. *Annu. Rev. Pharmacol. Toxicol.* **56**, 427–445 (2016).
5. Garinis, G. A. *et al.* Persistent transcription-blocking DNA lesions trigger somatic growth attenuation associated with longevity. *Nat. Cell Biol.* **11**, 604–615 (2009).
6. Barnhoorn, S. *et al.* Cell-autonomous progeroid changes in conditional mouse models for repair endonuclease XPG deficiency. *PLoS Genet.* **10**, e1004686 (2014).
7. Colman, R. J. *et al.* Caloric restriction delays disease onset and mortality in rhesus monkeys. *Science* **325**, 201–204 (2009).
8. Fontana, L., Partridge, L. & Longo, V. D. Extending healthy life span—from yeast to humans. *Science* **328**, 321–326 (2010).
9. Barzilai, N., Huffman, D. M., Muzumdar, R. H. & Bartke, A. The critical role of metabolic pathways in aging. *Diabetes* **61**, 1315–1322 (2012).
10. Speakman, J. R. & Mitchell, S. E. Caloric restriction. *Mol. Aspects Med.* **32**, 159–221 (2011).
11. Hoeijmakers, J. H. DNA damage, aging, and cancer. *N. Engl. J. Med.* **361**, 1475–1485 (2009).
12. López-Otín, C., Blasco, M. A., Partridge, L., Serrano, M. & Kroemer, G. The hallmarks of aging. *Cell* **153**, 1194–1217 (2013).
13. van der Pluijm, I. *et al.* Impaired genome maintenance suppresses the growth hormone–insulin-like growth factor 1 axis in mice with Cockayne syndrome. *PLoS Biol.* **5**, e2 (2007).
14. Wijnhoven, S. W. *et al.* Accelerated aging pathology in ad libitum fed *Xpd(TTD)* mice is accompanied by features suggestive of caloric restriction. *DNA Repair (Amst.)* **4**, 1314–1324 (2005).
15. Schumacher, B. *et al.* Delayed and accelerated aging share common longevity assurance mechanisms. *PLoS Genet.* **4**, e1000161 (2008).
16. Weeda, G. *et al.* Disruption of mouse ERCC1 results in a novel repair syndrome with growth failure, nuclear abnormalities and senescence. *Curr. Biol.* **7**, 427–439 (1997).
17. de Waard, M. C. *et al.* Age-related motor neuron degeneration in DNA repair-deficient *Ercc1* mice. *Acta Neuropathol.* **120**, 461–475 (2010).
18. Partridge, L. & Gems, D. Benchmarks for ageing studies. *Nature* **450**, 165–167 (2007).
19. Mair, W., Goymer, P., Pletcher, S. D. & Partridge, L. Demography of dietary restriction and death in *Drosophila*. *Science* **301**, 1731–1733 (2003).
20. Bogliolo, M. *et al.* Mutations in ERCC4, encoding the DNA-repair endonuclease XPF, cause Fanconi anemia. *Am. J. Hum. Genet.* **92**, 800–806 (2013).
21. Kashiwaga, K. *et al.* Malfunction of nuclease ERCC1-XPF results in diverse clinical manifestations and causes Cockayne syndrome, xeroderma pigmentosum, and Fanconi anemia. *Am. J. Hum. Genet.* **92**, 807–819 (2013).
22. Jaarsma, D., van der Pluijm, I., van der Horst, G. T. & Hoeijmakers, J. H. Cockayne syndrome pathogenesis: lessons from mouse models. *Mech. Ageing Dev.* **134**, 180–195 (2013).
23. Wilson, B. T. *et al.* The Cockayne Syndrome Natural History (CoSyNH) study: clinical findings in 102 individuals and recommendations for care. *Genet. Med.* **18**, 483–493 (2016).
24. Bartke, A., Sun, L. Y. & Longo, V. Somatotrophic signaling: trade-offs between growth, reproductive development, and longevity. *Physiol. Rev.* **93**, 571–598 (2013).
25. Gates, K. S. An overview of chemical processes that damage cellular DNA: spontaneous hydrolysis, alkylation, and reactions with radicals. *Chem. Res. Toxicol.* **22**, 1747–1760 (2009).
26. Swenberg, J. A. *et al.* Endogenous versus exogenous DNA adducts: their role in carcinogenesis, epidemiology, and risk assessment. *Toxicol. Sci.* **120** (Suppl. 1), S130–S145 (2011).
27. Borgesius, N. Z. *et al.* Accelerated age-related cognitive decline and neurodegeneration, caused by deficient DNA repair. *J. Neurosci.* **31**, 12543–12553 (2011).
28. Raj, D. D. *et al.* Priming of microglia in a DNA-repair deficient model of accelerated aging. *Neurobiol. Aging* **35**, 2147–2160 (2014).
29. Stranahan, A. M. & Mattson, M. P. Metabolic reserve as a determinant of cognitive aging. *J. Alzheimers Dis.* **30** (Suppl. 2), S5–S13 (2012).
30. Halagappa, V. K. *et al.* Intermittent fasting and caloric restriction ameliorate age-related behavioral deficits in the triple-transgenic mouse model of Alzheimer's disease. *Neurobiol. Dis.* **26**, 212–220 (2007).

Supplementary Information is available in the online version of the paper.

Acknowledgements We thank P. de With, J. Rigtens, E. Haasdijk, S. Gabriels, E. J. M. Stynenbosch, N. van Vliet, Y. van Loon, J. Baan and the animal caretakers for general assistance with mouse experiments. We thank A. H. J. Danser and J. P. van Leeuwen for support. We acknowledge financial support from the National Institute of Health (NIH)/National Institute of Ageing (NIA) (1P01 AG-17242-02), the National Institute for Public Health and the Environment and the Ministry of Health, Welfare and Sport of The Netherlands (S/340005), European Research Council Advanced Grant DamAge and Proof of Concept Grant Dementia to J.H.J.H., the European commission FP7 Markage (FP7-Health-2008-200880), DNA Repair (LSHG-CT-2005-512113), EU ITN Address (GA-316390), the KWO Dutch Cancer Society (5030), the Dutch CAA Foundation and the Royal Academy of Arts and Sciences of the Netherlands (academia professorship to J.H.J.H.). The research leading to these results has received funding from the European Community's Seventh Framework Programme (FP7/2007-2013) under grant agreement number HEALTH-F2-2010-259893. The funders had no role in study design, data collection and analysis, decision to publish, or preparation of the manuscript.

Author Contributions W.P.V., M.E.T.D., E.R., J.V., H.v.S., and J.H.J.H. designed the research and wrote the manuscript. D.J., C.P.-G., A.J.M.R., S.M.B., B.C.v.d.E., A.d.B., Á.G., and J.P. contributed to editing the manuscript. W.P.V., M.E.T.D., E.R., R.M.C.B., and S.B. performed and analysed the mouse lifespan cohorts. E.R., B.N., C.T.v.O., R.M.C.B., S.B., and S.I. performed genotyping and coordinated animal sectioning. S.A.Y., R.V.K., and A.d.B. assessed the ageing pathology characteristics. R.V.K. and S.I. performed FACS analysis of nuclei. S.M.B. and B.C.E. quantified bone changes. H.W. and A.J.M.R. quantified vascular function. C.R.B. performed the immunological analyses. W.P.V., D.J., R.M.C.B., and S.B. performed and analysed phenotypical scoring and behavioural analysis. W.P.V. and D.J. characterized neuropathological changes. W.P.V., E.R., C.P.-G., C.T.v.O., J.L.A.P., Á.G., and J.P. performed transcriptomic analyses and analysed the data. W.P.V., M.E.T.D., E.R., C.T.v.O., R.M.C.B., S.B., and S.I. performed the molecular studies.

Author Information The expression data have been deposited to the Gene Expression Omnibus database under accession number GSE77495. Reprints and permissions information is available at www.nature.com/reprints. The authors declare no competing financial interests. Readers are welcome to comment on the online version of the paper. Correspondence and requests for materials should be addressed to M.E.T.D. (martijn.dolle@rivm.nl) or J.H.J.H. (j.hoeijmakers@erasmusmc.nl).

Reviewer Information *Nature* thanks C. Lopez-Otin, M. Mattson and the other anonymous reviewer(s) for their contribution to the peer review of this work.

METHODS

Mouse models. The generation and characterization of *Ercc1*^{Δ/+} and *Ercc1*^{Δ/-} mice have been previously described¹⁶. *Ercc1*^{Δ/-} mice were obtained by crossing *Ercc1*^{Δ/+} (in a pure C57BL6J or FVB background) with *Ercc1*^{+/-} mice (in a pure FVB or C57BL6J background respectively) to yield *Ercc1*^{Δ/-} offspring with a genetically uniform F1 C57BL6J/FVB hybrid background (see ref. 6 for motivation). Wild-type F1 littermates were used as controls. *Xpg*^{-/-} mice have been characterized previously⁶ and were generated by crossing *Xpg*^{+/-} (in a pure C57BL6J background) with *Xpg*^{+/-} mice (in a pure FVB background). Hence, all animals used in the studies described here were of the same F1 C57BL6J/FVB hybrid background. Typical unfavourable characteristics, such as blindness in an FVB background or deafness in a C57BL6J background, do not occur in this hybrid background.

Mice were weighed, visually inspected weekly, and scored in a blinded fashion for gross morphological and motor abnormalities. Since the *Ercc1*^{Δ/-} and *Xpg*^{-/-} mice were smaller, food was administered within the cages and water bottles with long nozzles were used from around two weeks of age. Animals were maintained in a controlled environment (20–22 °C, 12 h light:12 h dark cycle) and were housed in individual ventilated cages under specific pathogen free conditions. Animals were individually housed at the EMC location and group housed at the RIVM location. Experiments were performed in accordance with the Principles of Laboratory Animal Care and with the guidelines approved by the Dutch Ethical Committee in full accordance with European legislation.

For the lifespan studies the indicated number of mice per group for *ad libitum* and 30% dietary restriction were generated. Additionally, several cross-sectional cohorts were generated. For *Ercc1*^{Δ/-} mice we generated groups which were killed at 7, 11, 16 or 30 weeks of age. The 7-week group consisted only of *ad libitum*-fed animals while the 30-week group consisted only of dietary restriction-treated mice. For wild-type mice, *ad libitum*-fed and dietary restriction-treated groups were sacrificed at 11, 16 or 20 weeks. Sample size of the lifespan cohorts were based on power analysis. No statistical methods were used to predetermine sample size of cross-sectional cohorts. Animals were divided randomly over all groups to prevent selection bias. All mice were clinically diagnosed daily in a blinded manner and, when moribund, killed, after which necropsy was performed. Animals from cross-sectional cohorts were killed when necropsy age was reached. Organs were stored at -80 °C for molecular analysis or (perfusion) fixated in (para) formaldehyde for pathological examinations. Statistics was performed with survival curve analysis using the product-limit method of Kaplan and Meier in GraphPad Prism.

Diets. All animals were bred and maintained on AIN93G synthetic pellets (Research Diet Services B.V.; gross energy content 4.9 kcal/g dry mass, digestible energy 3.97 kcal/g). The initial lifespan cohort, shown in Fig. 1a, were fed standard AIN93G pellets containing 2.5 g/kg choline bitartrate. To avoid potential formation of bladder and kidney stones, we replaced choline bitartrate with choline chloride in all subsequent experiments. The amount of dietary restriction was determined in a prior pilot study and food intake of the *ad libitum*-fed mice was continuously monitored. On average, *Ercc1*^{Δ/-} and *Xpg*^{-/-} mice ate 2.3 g food per day. Dietary restriction was initiated at 7 weeks of age with 10% food reduction (2.1 g/day), when animals reached almost-maximum bodyweight and development was completed. Dietary restriction was increased weekly by 10%, until it reached 30% dietary restriction (1.6 g/day) from 9 weeks of age onward. Temporary dietary restriction was initiated directly with 30% food reduction at 6 weeks of age. These mice received *ad libitum* food again from 12 weeks onward. Wild-type mice ate on average 3.0 g food per day, resulting in 2.1 g/day for 30% dietary restriction. Food was given to the animals just before the start of the dark (active) period to avoid alteration of the biological clock.

Pathology assessment of ageing characteristics. Representative sections from the liver, kidneys, sciatic nerve, testes and femur were processed, stained with haematoxylin and eosin, and microscopically examined in a blinded manner by two board-certified pathologists (SAY, AdB) for the presence of histopathologic lesions. The severity score of lesions was semi-quantitatively assessed. Scores were given as absent (0), subtle (1), mild (2), moderate (3), severe (4), and massive (5). Digital images from the kidneys and femur cortical bone at mid-shaft area were taken for morphometric analysis using Labsense image analysis software (Olympus). Ageing characteristics were assessed in >5 animals per group per sex. Groups were compared with nonparametric Mann–Whitney U and Kruskal–Wallis tests.

FACS analysis of nuclear DNA content. Polyploidy levels were assessed based on propidium iodide (PI) fluorescence using FACS analysis^{31,32}. A small part of the left lobe (approximately 5 mm³) was dissected from *ad libitum*- and dietary restriction-treated *Ercc1*^{Δ/-} mice (7, 11, 16 and 30 weeks, *n* = 5) and wild-type mice (11 weeks, *n* = 5), cut into small fragments and suspended in 800 μl PBS

using a syringe (21G). 300 μl homogenate was added to 300 μl 100% ethanol for fixation. Samples were stored for at least 24 h before further processing. After fixation the liver homogenate was washed with ice-cold PBS and subsequently incubated with a pepsin solution for 20 min. After washing in PBS/Tween-20, cells were collected in 500 μl PBS supplemented with 5 μg/ml PI and 250 μg/ml RNase and samples were measured using the FACS (FACSCalibur, Becton Dickinson). Differences between groups were assessed with a two-way ANOVA, with age and diet as fixed factors.

Micro-computed tomographic (micro-CT) quantification of bone thickness. *Ad libitum*- and diet-restricted mice were killed by cervical dislocation at scheduled ages, femora were excised and non-osseous tissue was removed. Two days after fixation in 4% formalin, the right femora were scanned using Skyscan 1076 *in vivo* X-Ray computed tomography (Bruker microCT) with a voxel size of 8.88 μm. Osseous tissue was distinguished from non-osseous tissue by segmenting the reconstructed grayscale images with an automated algorithm using local thresholds³³. The region of interest (ROI) (the distal metaphysis of the femora) was selected using 3D data analysis software. To compensate for bone length differences, the length of each ROI was determined relative to the largest specimen femur of the cohort. The cortex and trabeculae of the metaphysis were separated using automated software developed in-house. The thickness of the trabeculae and cortices were assessed using 3D analysis software as described³⁴ using the CT analyser software package (Bruker microCT). A bone specimen with known bone morphometrics was included within each scan as a quantitative control. Statistical significance was calculated using one-way Anova with Bonferroni's multiple comparison test.

Ex vivo vascular function. The responses of isolated aortic tissue were *ex vivo* measured in small-wire myograph organ baths containing oxygenated Krebs-Henseleit buffer at 37 °C. After preconstriction with 30 nmol/l U46619, relaxation concentration–response curves to acetylcholine were constructed³⁵.

Immunological analyses. Single-cell suspensions were prepared from spleen by passing the cells through a cell strainer with HEPES-buffered saline solution (HBSS) supplemented with 2% FBS and washed. Erythrocytes were eliminated with ACK buffer. For CD4⁺CD25⁺Foxp3⁺ staining, cells were first stained for the expression of cell surface markers and then fixed, permeabilised, and stained using the Foxp3 kit (eBiosciences) according to the manufacturer's instructions. FACS analysis was performed using FACS (Becton Dickinson) and analysed with FlowJo Software (TreeStar).

Blood glucose, insulin and albumin levels. Mice were killed by CO₂ asphyxiation and blood was immediately collected from the heart. Glucose levels were measured using a Freestyle mini blood glucose metre. Insulin and albumin levels were measured in blood plasma using an ultrasensitive mouse insulin Elisa (Mercodia AB) or mouse albumin ELISA kit (Immunology Consultants Laboratory, Inc.), respectively. Insulin levels were determined after overnight fasting. Glucose levels were determined after feeding, at the beginning of the dark period.

IgA measurements. Euthanasia of moribund or cross-sectional animals was performed by intramuscular injection of a ketamine–rompun mixture, followed by exsanguination³. IgA immunoglobulin was measured in blood serum using the commercially available bead-based multiplexed panel Mouse Immunoglobulin Isotyping (Millipore Corporation). Standard analysis protocols were followed and all samples were analysed at least *in duplo*.

Phenotype scoring. The mice were weighed and visually inspected weekly, and were scored in a blinded manner by two experienced research technicians (R.M.C.B. and S.B.) for the onset of various phenotypical parameters. Clasping was measured by suspending mice by their tails for 20 s. A clasping event was scored when retraction of both hind limbs towards the body was observed for at least 5 s. Whole-body tremor was scored if mice were trembling for a combined total of at least 10 s when put on a flat surface for 20 s. Impaired balance was determined by observing the mice walking on a flat surface for 20 s. Mice that had difficulties in maintaining an upright orientation during this period were scored as having imbalance. If mice showed a partial loss of function of the hind limbs, they were scored as having paresis. Statistics were performed with survival-curve analysis using the product-limit method of Kaplan and Meier in GraphPad Prism.

Behavioural analyses. Rotarod performance was assessed by measuring the average time spent on an accelerating rotarod (Ugo Basile). All animals were given four consecutive trials of a maximum of 5 min with inter-trial intervals of 1 h. For weekly monitoring, the motor coordination performance was measured with two consecutive trials of a maximum of 5 min. Grip strength was determined by placing mice with forelimbs or all limbs on a grid attached to a force gauge, and steadily pulling the mice by their tail. Grip strength is defined as the maximum strength produced by the mouse before releasing the grid. For each value the test was performed in triplicate.

TUNEL staining. To quantify apoptotic cells in the retina, eyes were fixed overnight in 10% phosphate-buffered formalin (JT Baker), paraffin-embedded, sectioned at 5 mm, and mounted on Superfrost Plus slides. Paraffin sections were employed for TdT-mediated dUTP nick-end labelling (TUNEL) assay using an Apoptag Plus Peroxidase *in situ* apoptosis detection kit (Millipore). Sections were deparaffinised and incubated as described by the manufacturer. Statistical differences were calculated with a *t*-test.

Antibodies. Primary antibodies (supplier; catalogue number; dilutions) used in this study were as follows: rabbit anti-ATF3 (Santa Cruz; sc-188; 1:2,000), goat anti-ChAT (Millipore; AB144P; 1:500); rabbit anti-GFAP (DAKO; Z0334; 1:8,000); mouse anti-GM130 (BD Transduction; 610823; 1:100); rabbit anti-Iba-1 (Wako; 019-19741; 1:5,000); rat anti-Mac2 (Cedarlane; CL8942AP; 1:2,000); mouse anti-NeuN (Millipore; MAB377; 1:1,000); rabbit anti-p53 (Leica; NCL-p53-CM5p; 1:1,000); mouse anti- γ H2AX (Millipore; 05-636; 1:4,000). For avidin-biotin-peroxidase immunocytochemistry biotinylated secondary antibodies from Vector Laboratories, diluted 1:200 were used. Alexa488-, Cy3-, and Cy5-conjugated secondary antibodies raised in donkey (Jackson ImmunoResearch) diluted at 1:200 were used for confocal immunofluorescence.

Histological procedures. Mice were anaesthetized with pentobarbital and perfused transcardially with 4% paraformaldehyde. The brain and spinal cord were carefully dissected out, post-fixed for 1 h in 4% paraformaldehyde, cryoprotected, embedded in 12% gelatin, rapidly frozen, and sectioned at 40 μ m using a freezing microtome or stored at -80°C until use. Frozen sections were processed free floating using the ABC method (ABC, Vector Laboratories) or single-, double-, and triple-labelling immunofluorescence. Immunoperoxidase-stained sections were analysed and photographed using an Olympus BX40 microscope. Immunofluorescence sections were analysed using a Zeiss LSM700 confocal microscope. Mean intensities were quantified using Fiji. Statistical differences were calculated with a *t*-test.

RNA isolation. Total RNA was extracted using QIAzol lysis Reagent from mouse tissue specimens. For increased purity, miRNAeasy Mini Kits (QIAGEN) were used. Addition of wash buffers RPE and RWT (QIAGEN) was done mechanically by using the QIAcube (QIAGEN) via the miRNeasy program and tissue was stored at -80°C . The concentration of RNA was measured by Nanodrop (Thermo Fisher Scientific).

Real-time PCR. Gene expression analyses were performed with gene-specific real-time PCR primers (see below) using SYBR Green (Sigma-Aldrich) and Platinum Taq polymerase (Life Technologies) on a Bio-Rad CFX96 thermocycler or with pre-designed TaqMan Gene Expression Assays (given below) with a 7500 Fast Real-Time PCR System (Applied Biosystems). Relative gene expressions were calculated as previously described⁶. For SYBR Green method the following primers were used (forward primer 5' to 3'; reverse primer 5' to 3'): Gsta1 (CTTCTGACCCTTCCCTCT; ATCCATGGGAGGCTTTCTCT), Nqo1 (GGTAGCGCTCCATGTACT; GAGTGTGGCCAATGCTGTAA), Nfe2l2 (AGGACATGGAGCAAGTTTGG; TCTGTCACTGTGGCTTCTGG), Gsta2 (CGAGCAATTCTCCAGGTGA; TATTCGTGGACTTGGGCACG), Fkbp5 (TGTTCAAGAAGTTCGCAGAGC; CCTTCTTGCTCCCAGCTTT), Srxn1 (TGAGCAGCTCTCTGATGTG; GCTGAGGTGACAATTGACTATGG), Gsta4 (TCGATGGGATGATGCTGAC; CATCTGCATACATGCTCAATCCTG), Gclm (TGGAGCAGCTGTATCAGTGG; CAAAGGCAGTCAAATCTGGTG), Hmox1 (CAGGTGATGCTGACAGAGGA; ATGGCATAAATCCCAGTGC), Gclc (AGATAGTAGAACACGGGAGGAG; TGATCCTAAAGCGATTGTCTTC), Epxh1 (GAGTGGAGGAACCTGCACAC; AGCAGAGAAGCCAGGATGA), Mgst1 (CTCGGCAGGCAACTCTGC; CCATGCTTCCAATCTTGGTC), Tubg2 (CAGACCAACCACTGCTACAT; AGGGAATGAAGTTGGCCAGT), Hprt (TGATAGATCCATTCCTATGACTGTAGA; AAGACATTCTTCCAGTTAAAGTTGAG), Rps9 (ATCCGCCAACGTCACATTA; TCTTCACTCGGCCCTGAC). As pre-designed TaqMan assays we used (order number; sequence 5' to 3'): Ghr (Mm00439093_m1; GACAAGCTGCAAGAATTGCTCATGA), Igflr (Mm00802831_m1; GGCCAGAAGTGGAGCAGAATAATCT), HPRT-E2_3 (HPRT-E2_3_F; GCCGAGGATTTGGAAAAAGTGTTTA, HPRT-E2_3_R; TTCATGACATCTCGAGCAAGTCTTT, HPRT-E2_3_M; CAGTCTGTCCA TAATCA), POLR2A-E2_3 (POLR2A-E2_3F; GCAGTTCGGAGTCTCTGAGT, POLR2A-E2_3R; CCTCTGTTGTTTCTGGGATTTGA, POLR2A-E2_3M2; CATCCGCTTCAATTCAT).

Microarray hybridizations. RNA quality was assessed using the 2100 Bio-Analyzer (Agilent Technologies) following the manufacturer's instructions. The quality of the RNA is expressed as the RNA integrity number (RIN, range 0–10). Samples with a RIN below 8 were excluded from analysis. Hybridization to Affymetrix HT MG-430 p.m. Array Plates was performed at the Microarray Department of the University of Amsterdam according to Affymetrix protocols. Quality control and normalization were performed using the pipeline at the www.arrayanalysis.org website (Maastricht University).

miRNA expression. The same total RNA extracts were used as extracted for mRNA analysis (above). miRNA expression levels were assessed using a miRNA micro-array (miRCURY LNA microRNA Array (7th Gen.), Exiqon). All probes with more than three calls were selected for assessing differential expression between groups. Differences in mean expression were compared using a one-way ANOVA. Probes with a FDR of 5% were considered as significantly differentially expressed.

Total RNA-seq. RNA expression analysis was also performed with the next-generation sequencing approach on one animal per treatment as described in ref. 36.

Data pre-analysis. Raw data (CEL files) were normalized by robust multichip average (RMA) in the oligo BioConductor package, which summarizes perfect matches through median polish and collapses probes into core transcripts based on CDF annotation file provided by Affymetrix using the R open statistical package (<http://www.r-project.org/>). All data files have been submitted to the NCBI gene expression omnibus under accession number GSE77495.

Principal component analysis. Principal component analysis (PCA) was performed using all the probe sets in the array. A graphical representation was generated to show the relationship among the different samples. PCA is a linear projection method that defines a new dimensional space to capture the maximum information present in the initial data set. It is an unsupervised exploratory technique used to remove noise, reduce dimensionality and identify common/dominant signals oriented to try to find biological meaning³⁷. The two principal components with the highest amount of variance were plotted. PCA was performed using the prcomp package and the plot was drawn with gplots, both from the Bioconductor project (<https://www.bioconductor.org/>).

Detection of differentially expressed genes (DEG). The linear model from Limma³⁸ implemented in R was used to identify the DEGs. Pairwise comparisons for each genotype between ad libitum and dietary restriction samples were applied to calculate the fold change (FC), *P* value and false discovery rate (FDR) for each probe in the microarray. Cut-off values for a DEG were put at FDR < 5% with FC \geq |1.5|. For all mouse analyses, differentially expressed probes were considered as DEGs.

Determination of enrichment factor and *P* values of overlap. Overlap between lists of DEGs was identified looking by the intersection between pair of lists. To determine if the overlap was higher than expected by chance the hypergeometric distribution was used as is implemented in phyper function in R. Additionally the factor of enrichment was calculated with the formula: $EF = nAB / ((nA \times nB) / nC)$. Where: nA = Number of DEG in experimental group A; nB = Number of DEG in experimental group B; nC = Number of total genes in the microarray; nAB = Number of common DEG between A and B.

Pathway analysis. Pathway enrichment analysis was conducted via overrepresentation analysis (ORA). ORA was performed in the Interactive pathway analysis (IPA) of complex genomics data software (Ingenuity Systems, Qiagen) by employing a pre-filtered list of differentially expressed genes. Genes were selected as differentially expressed if they had a fold change \geq 1.5 and an FDR lower than 0.05. The over-represented canonical pathways were generated based on information in the Ingenuity Pathways Knowledge Base. A pathway was selected as deregulated when the *P* value in the Fisher test was lower than 0.01.

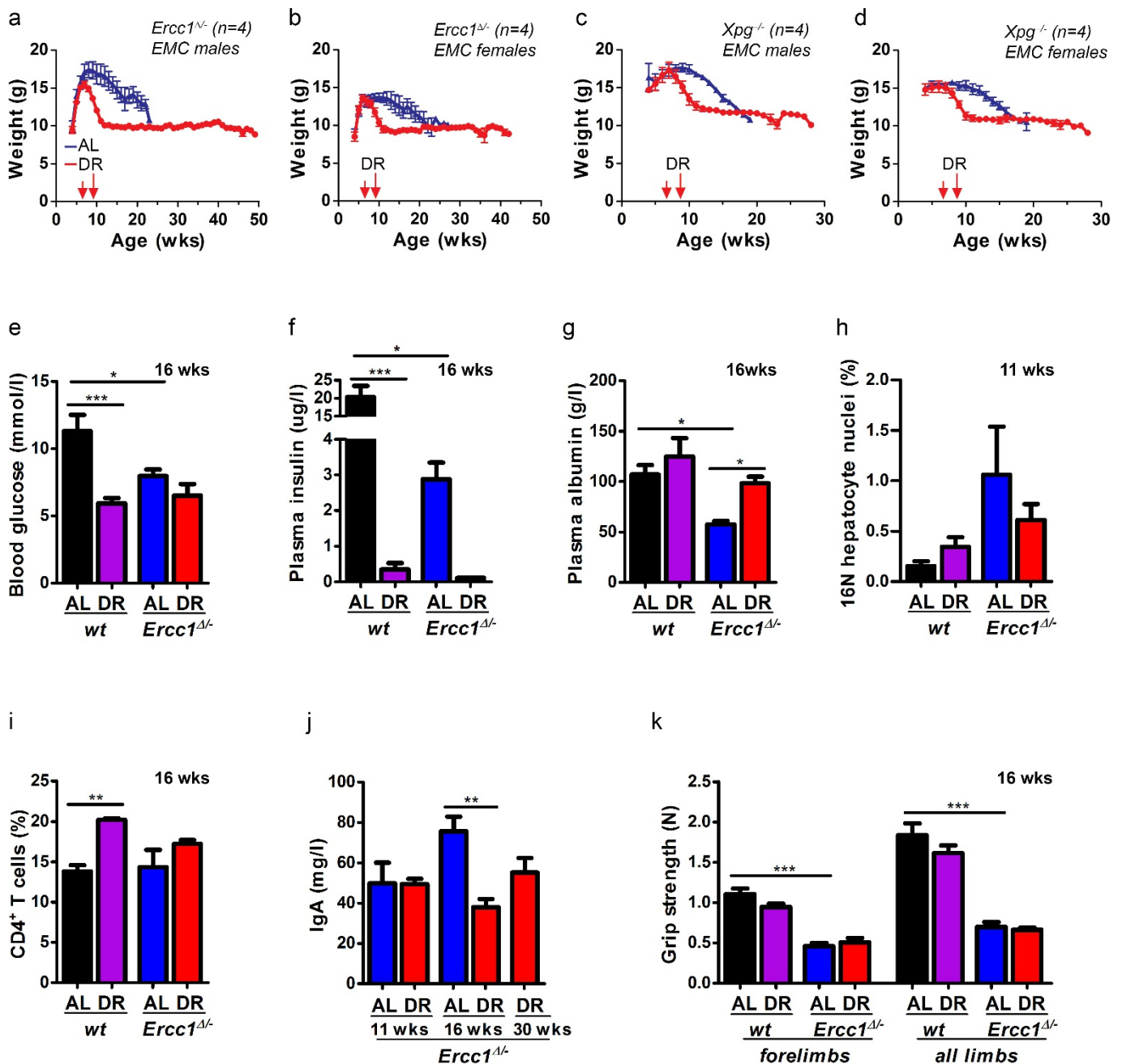
Additionally, IPA transcription factor (TF) analysis was performed to identify the cascade of upstream transcriptional regulators that can explain the observed gene expression changes in the different lists of DEGs. To do this, data stored in the Ingenuity Knowledge Base, with prior information on the expected effects between TF and their target genes, were used. The analysis examines how many known targets of each TF are present in the list of DEGs, and also compares their direction of change to what is expected from the literature, in order to predict likely relevant transcriptional regulators. If the observed direction of change is mostly consistent with a particular activation state of the transcriptional regulator ('activated' or 'inhibited'), then a prediction is made about that activation state. For each TF two statistical measures are computed (overlap *P* value and activation *z*-score). The overlap *P* value labels upstream regulators based on significant overlap between data set genes and known targets regulated by a TF. The activation *z*-score is used to infer the likely activation states of upstream regulators based on comparison with a model that assigns random regulation directions. Overlap *P* value lower than 0.05 and *z*-score higher than |2| were selected as thresholds to identify a TF as relevant.

Gene length analysis. Limma was used to identify the DEGs among AL^{WT} samples compared with the other experimental conditions (DR^{WT}, AL^{Erc1} and DR^{Erc1}). Next, probe-sets in the Affymetrix array with multiple gene annotation were filtered out. BiomaRt³⁹ was used to retrieve the gene length for the remaining probe sets (32,930 probe-sets from 45,142 probe-sets in the original microarray). Differentially expressed genes were selected using an FDR of <0.05 and a linear

fold change of ± 1.5 . The Shapiro–Wilk test was applied to contrast the normality of the distribution of gene length in the different lists of DEGs. Because most of the distributions were not normal, a Mann–Whitney test for non-paired samples test was used to evaluate whether the distributions of DEGs were different between the different comparisons. Finally, a relative frequency (kernel density) plot of gene length and probability density for DEG in each comparison was drawn using the density function implemented in R. Kernel density estimates are related to histograms, but with the possibility to smooth and continuity by using a kernel function. The y axis represents the density probability for a specific range of values in the x axis.

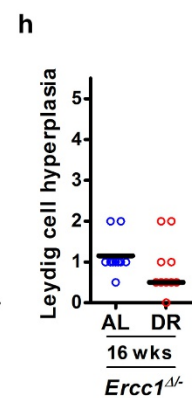
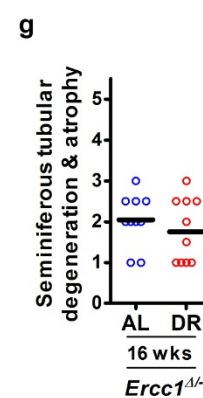
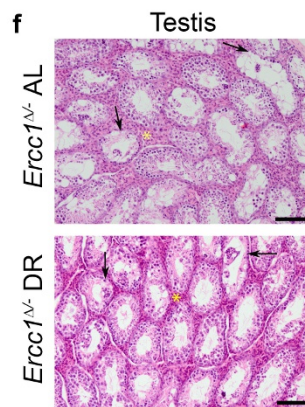
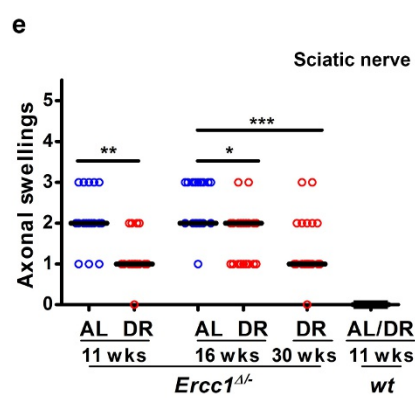
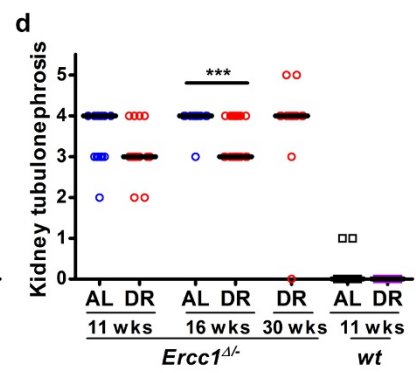
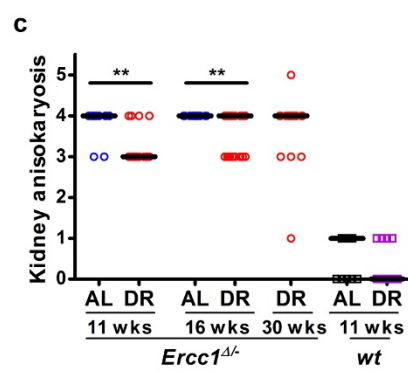
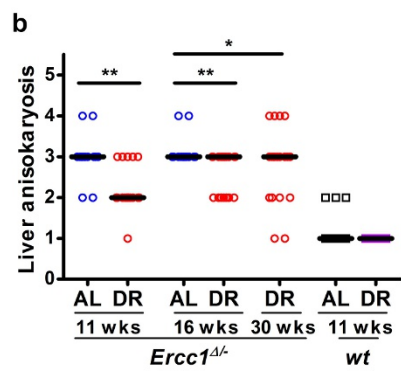
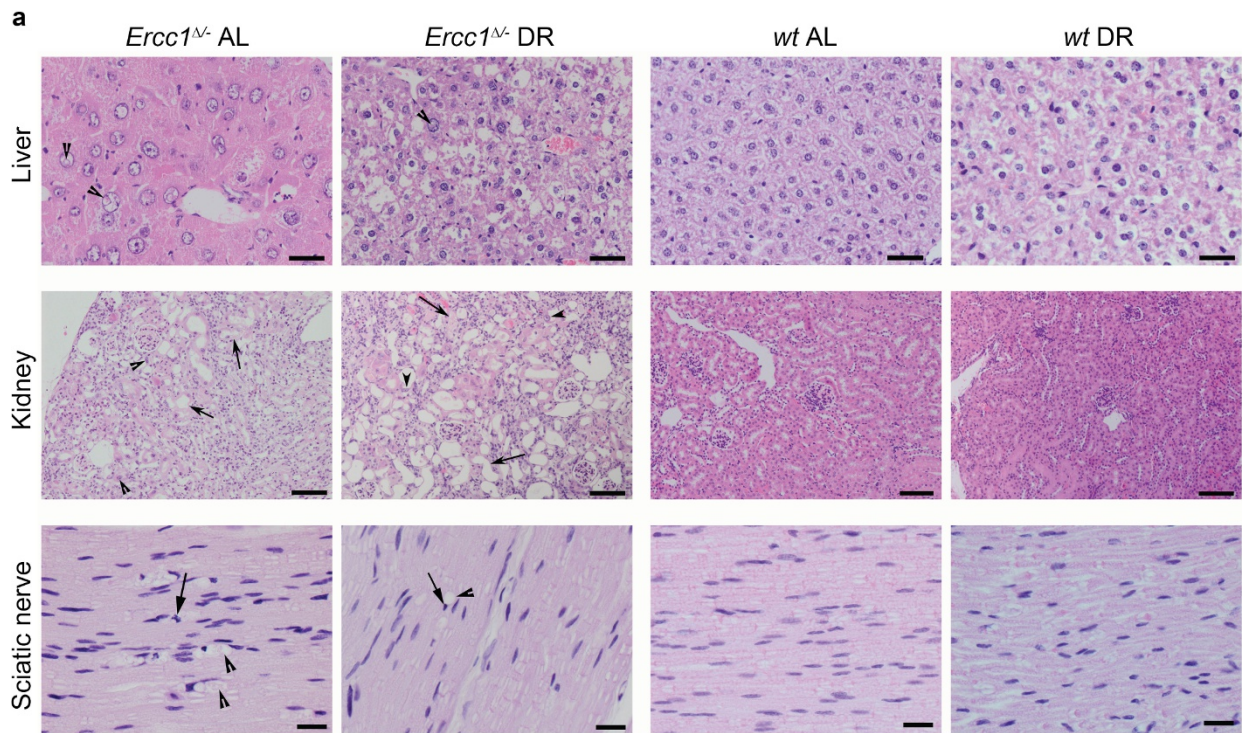
Immunoblotting. Liver extracts from *ad libitum*- and dietary restriction-treated *Erc1 Δ* ^{-/-} and wild type mice ($n = 6$, 11 weeks) were prepared by mechanical disruption in lysis buffer (150 mM NaCl, 1% Triton X-100, 50 mM Tris), which was supplemented with mini complete protease inhibitor (Roche Diagnostics) and phosphate inhibitors (5 mM NaF, 1 mM Na-orthovanadate). After mechanical disruption, lysates were incubated on ice for 1 h and subsequently centrifuged at 4 °C for 20 min. Lysate (25–50 μ g) was loaded on a 10% SDS–PAGE gel (Life Technologies LTD) and transferred to a PVDF transfer membrane (GE-Healthcare Life Sciences). Levels of S6 (#2217S Lot5; 1:2,000), S6(Ser240/244; #2215 Lot14; 1:500), Akt (#9272 Lot25; 1:500), Akt(Ser473; #9271S Lot13; 1:250) and Akt(Thr308; #9275S Lot19; 1:500) were detected (Cell Signaling Technology), semi-quantified using the ImageJ software package (<http://rsb.info.nih.gov/ij/index.html>) and phosphorylated:total ratios relative to *ad libitum* samples were calculated. Differences between groups were assessed with a t -test. β -Actin was used as loading control (Sigma; A5441 Lot064M4789V; 1:25,000).

31. Duncan, A. W. *et al.* The ploidy conveyor of mature hepatocytes as a source of genetic variation. *Nature* **467**, 707–710 (2010).
32. McWhir, J., Selfridge, J., Harrison, D. J., Squires, S. & Melton, D. W. Mice with DNA repair gene (ERCC-1) deficiency have elevated levels of p53, liver nuclear abnormalities and die before weaning. *Nat. Genet.* **5**, 217–224 (1993).
33. Waarsing, J. H., Day, J. S. & Weinans, H. An improved segmentation method for in vivo microCT imaging. *J. Bone Miner. Res.* **19**, 1640–1650 (2004).
34. Botter, S. M. *et al.* ADAMTS5^{-/-} mice have less subchondral bone changes after induction of osteoarthritis through surgical instability: implications for a link between cartilage and subchondral bone changes. *Osteoarthritis Cartilage* **17**, 636–645 (2009).
35. Durik, M. *et al.* Nucleotide excision DNA repair is associated with age-related vascular dysfunction. *Circulation* **126**, 468–478 (2012).
36. Derks, K. W. *et al.* Deciphering the RNA landscape by RNAome sequencing. *RNA Biol.* **12**, 30–42 (2015).
37. Ringnér, M. What is principal component analysis? *Nat. Biotechnol.* **26**, 303–304 (2008).
38. Smyth, G. K., Gentleman, R., Carey, V., Dudoit, S., Irizarry, R. & Huber, W. (eds.), *Bioinformatics and Computational Biology Solutions Using R and Bioconductor pp. 397–420* (Springer, 2005).
39. Durinck, S., Spellman, P. T., Birney, E. & Huber, W. Mapping identifiers for the integration of genomic datasets with the R/Bioconductor package biomaRt. *Nat. Protocols* **4**, 1184–1191 (2009).
40. Jonker, M. J. *et al.* Life spanning murine gene expression profiles in relation to chronological and pathological aging in multiple organs. *Aging Cell* **12**, 901–909 (2013).
41. de Graaf, E. L. *et al.* Spatio-temporal analysis of molecular determinants of neuronal degeneration in the aging mouse cerebellum. *Mol. Cell. Proteomics* **12**, 1350–1362 (2013).
42. He, L. *et al.* A microRNA component of the p53 tumour suppressor network. *Nature* **447**, 1130–1134 (2007).
43. Navarro, F. & Lieberman, J. miR-34 and p53: new insights into a complex functional relationship. *PLoS One* **10**, e0132767 (2015).
44. Swindell, W. R. Genes and gene expression modules associated with caloric restriction and aging in the laboratory mouse. *BMC Genomics* **10**, 585 (2009).
45. Campisi, J. & Robert, L. Cell senescence: role in aging and age-related diseases. *Interdiscip. Top. Gerontol.* **39**, 45–61 (2014).
46. Coppé, J. P., Desprez, P. Y., Krtolica, A. & Campisi, J. The senescence-associated secretory phenotype: the dark side of tumor suppression. *Annu. Rev. Pathol.* **5**, 99–118 (2010).



Extended Data Figure 1 | Effect of dietary restriction on body weight and various healthspan parameters of *Ercc1*^{Δ/Δ} mice are primarily related to glucose metabolism and liver pathology. a–d, Body weight curves of *Ercc1*^{Δ/Δ} (a, b) and *Xpg*^{-/-} (c, d) male (a, c) and female (b, d) mice with *ad libitum* (blue) access to AIN93G diet or on 30% dietary restriction (red) shown as mean ± s.e. at weekly intervals; n = 4 animals per group, solitary housed at the EMC. Dietary restriction was initiated at 7 weeks of age at a restriction of 10% and increased weekly by 10%, until 30% was reached from 9 weeks of age onwards. e–g, Blood glucose after feeding (e), plasma fasting insulin (f), and plasma albumin levels (g), indicative of liver functioning, in *ad libitum* and dietary restriction wild-type and *Ercc1*^{Δ/Δ} mice at 16 weeks. n ≥ 3 animals per group.

h, Quantification of 16N nuclei in hepatocytes³² of 11-week-old male wild-type and *Ercc1*^{Δ/Δ} mice under *ad libitum* or dietary restriction regimens by FACS analyses; n = 5 animals per group. i, Total numbers of splenic CD4⁺ T cell from spleen of 16-week old *Ercc1*^{Δ/Δ} mice under dietary restriction or *ad libitum* and aged-matched wild-type controls. n ≥ 3 animals per group. j, IgA blood levels in male *Ercc1*^{Δ/Δ} mice at different ages under dietary restriction or *ad libitum* regimes. n = 5 animals per group. k, Average grip strength of the forelimbs and all limbs of 16-week old *Ercc1*^{Δ/Δ} and wild-type mice is similar under *ad libitum* and dietary restriction conditions; n = 4 animals per group. Mean ± s.e. *P < 0.05, **P < 0.01, ***P < 0.001.

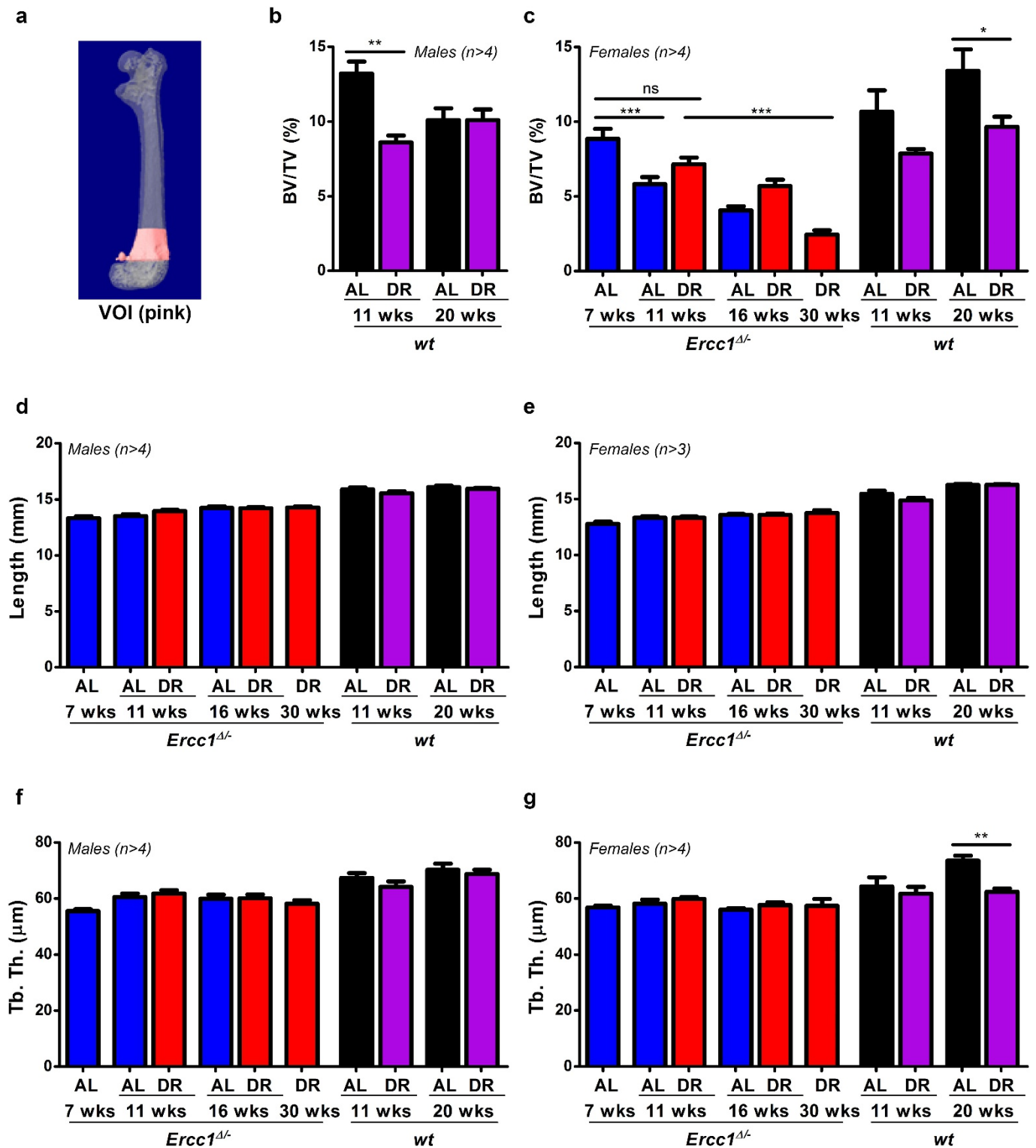


Extended Data Figure 2 | See next page for caption.

Extended Data Figure 2 | Dietary restriction improves ageing-related histopathological phenotypes in different tissues of *Ercc1*^{Δ/−} mice.

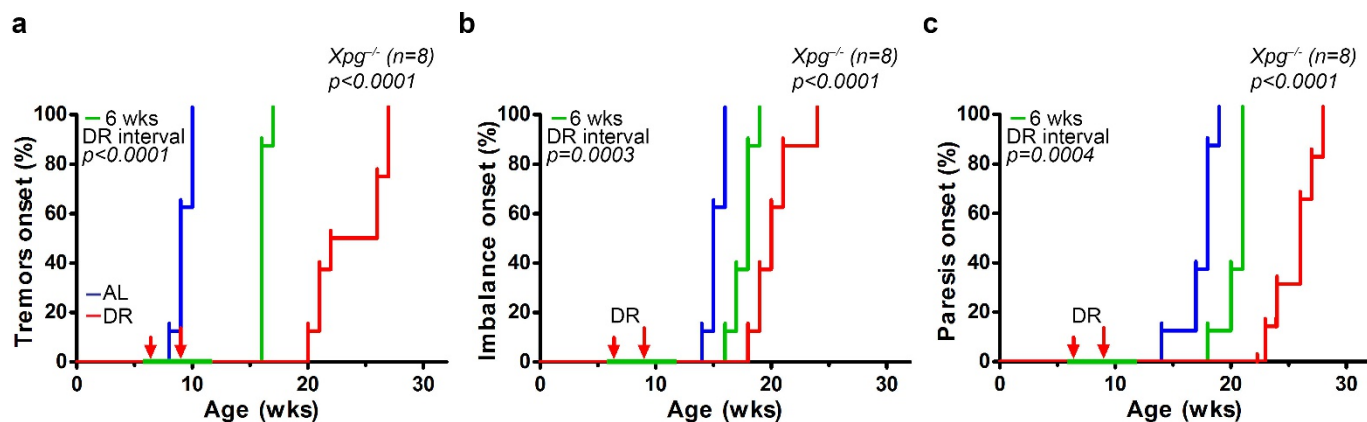
a, Representative pictures of haematoxylin-eosin-stained slides from liver, kidney, and sciatic nerve. From left to right: AL^{Ercc1}, DR^{Ercc1}, AL^{WT} and DR^{WT}. Lesions were semiquantitatively assessed, with scores ranging from absent (0) to massive (5). The liver of a female AL^{Ercc1} mouse shows moderate anisokaryosis (score = 3) and intranuclear inclusions (score = 3, arrowheads). The liver of a female DR^{Ercc1} mouse shows moderate hydropic degeneration with mild anisokaryosis (score = 1) and a few hepatocellular intranuclear inclusions (score = 1, arrowhead). Histologically normal liver tissue from AL^{WT} and DR^{WT} mice. The kidney of a female AL^{Ercc1} and DR^{Ercc1} mouse with severe tubular attenuation and degeneration (score = 5, arrows) with marked anisokaryosis (score = 4, arrowheads) next to histologically normal kidneys from female AL^{WT} and DR^{WT} mice. The sciatic nerve of a female AL^{Ercc1} mouse with severe axonal swellings (score = 3, arrowheads). These axonal swellings probably represent vacuoles containing myelin debris and/or fragmented axons. The Schwann cell nuclei around vacuolated areas are pyknotic (arrow). The sciatic nerve of a female DR^{Ercc1} mouse displays mild vacuole-like structures (score = 1, arrowhead) with pyknosis of Schwann cell nuclei (arrow), while the histologically normal sciatic nerves of female AL^{WT} and DR^{WT} mice display no axonal swellings. Scale bar in liver, 50 μm; in kidney, 100 μm; in sciatic nerve, 20 μm. **b**, Pathology assessment of anisokaryosis in livers from *Ercc1*^{Δ/−} mice at different ages under *ad libitum* (blue) or dietary restriction (red) regimen and young *ad libitum* (black) and dietary restriction (purple) wild-type controls. Scores range from absent (0) to

massive (5); $n \geq 10$ animals per group; bars indicate group medians. **c, d**, Pathology assessment of anisokaryosis (**c**) and tubulonephrosis (**d**) in the kidneys of *Ercc1*^{Δ/−} and wild-type mice at different ages under *ad libitum* and dietary restriction regimes. Scores range from absent (0) to massive (5); $n \geq 10$ animals per group. **e**, Pathology assessment of axonal swellings in sciatic nerves of *Ercc1*^{Δ/−} mice at different ages under *ad libitum* or dietary restriction regimens. Scores range from absent (0) through massive (5); $n \geq 10$ animals per group. **f**, Representative pictures to the testicular lesions observed in *Ercc1*^{Δ/−} males. The AL^{Ercc1} testes (upper panel) exhibited moderate testicular degeneration and atrophy (arrows). Also, the Leydig cells (yellow asterisk) appeared more prominent, probably owing to the tubular loss and attenuation, or possibly owing to true Leydig cell hyperplasia (a common ageing lesion in rodent testes). These phenotypes were slightly rescued in the testes of DR^{Ercc1} mice (lower panel). **g, h**, Pathology assessment of seminiferous tubular degeneration and atrophy (**g**) and Leydig cell hyperplasia (**h**) in the testes of *Ercc1*^{Δ/−} mice at 16 weeks of age under *ad libitum* (blue) or dietary restriction (red) regimen. Scores were given as absent (0), subtle (1), mild (2), moderate (3), severe (4), and massive (5) for each criteria, with a 0.5 interval; $n = 10$ animals per group; bars indicate group medians. Note that testicular development is mostly completed at the start of dietary restriction. * $P < 0.05$, ** $P < 0.01$, *** $P < 0.001$. The values for the wild-type mice do not change significantly in the timeframes used here (see ref. 40). Pathological scores, including those of other liver and kidney ageing-related histopathological phenotypes, are given in Supplementary Table 1.



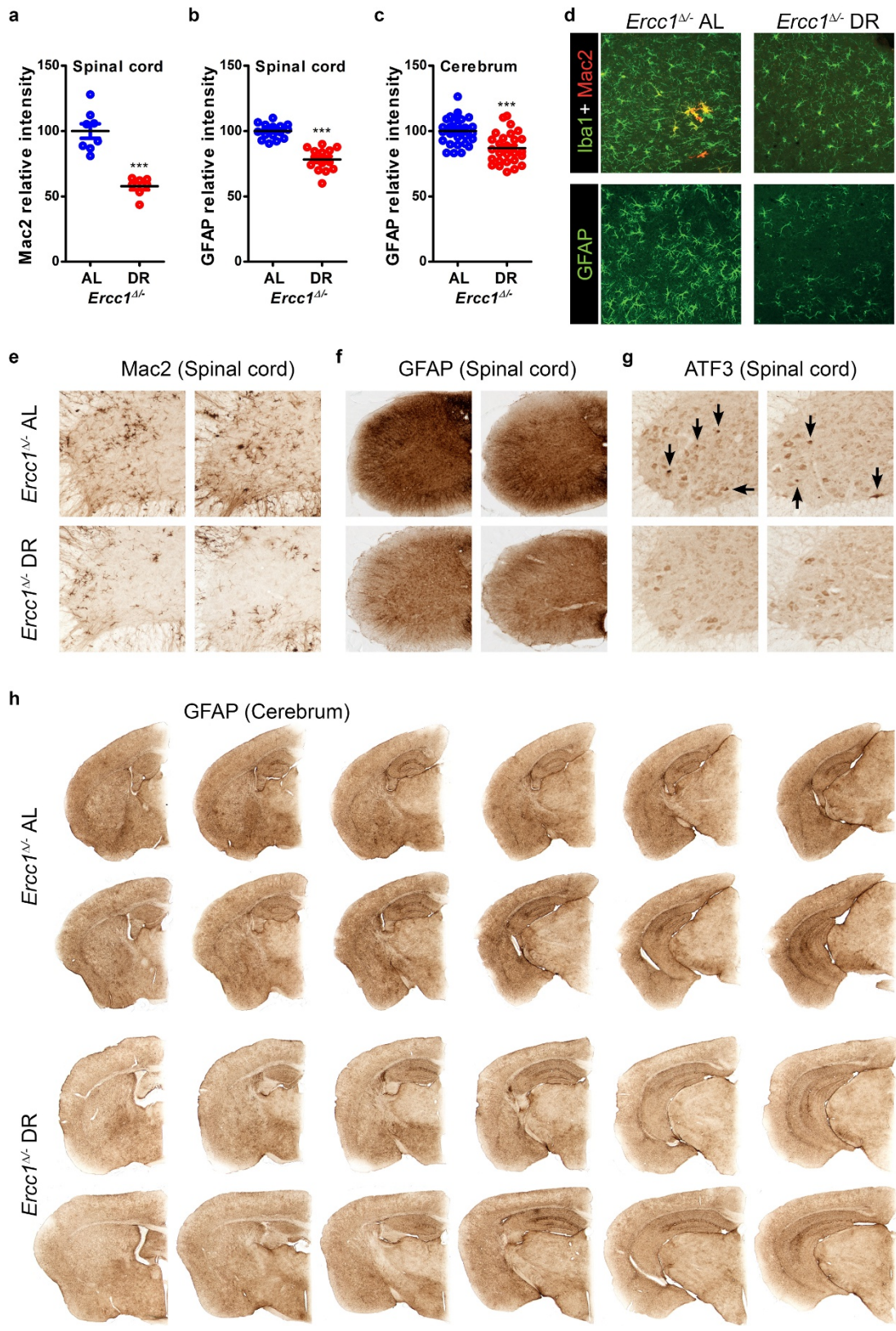
Extended Data Figure 3 | Dietary restriction preserves skeletal structure in *Ercc1*^{Δ/Δ} mice. **a**, Illustration depicting the femoral volume of interest (VOI) for microCT analyses. **b, c**, Trabecular bone volume fraction (BV/TV) representing the amount of trabecular bone in the femur VOI of wild-type male mice (**b**) as well as *Ercc1*^{Δ/Δ} and wild-type female mice (**c**) expressed as percentage measured using micro-CT. **d, e**, Femur length of *Ercc1*^{Δ/Δ} and wild-type male (**d**) and female (**e**) mice.

f, g, Trabecular thickness in the femur VOI of *Ercc1*^{Δ/Δ} and wild-type male (**f**) and female (**g**) mice. *Ad libitum*- and dietary restriction-treated animals were measured at different ages with $n \geq 3$ animals per group. Values of *Ercc1*^{Δ/Δ} mice are depicted in blue (*ad libitum*) and red (dietary restriction). Young wild-type controls are depicted in black (*ad libitum*) and purple (dietary restriction). Error bars denote mean \pm s.e. * $P < 0.05$, ** $P < 0.01$, *** $P < 0.001$.



Extended Data Figure 4 | Dietary restriction preserves neurofunctional behaviour of $Xpg^{-/-}$ mice. a–c, Onset of neurological abnormalities as tremors (a), imbalance (b), and paresis of the hind limbs (c) with age in $Xpg^{-/-}$ mice under *ad libitum* and dietary restriction regimens. $n = 8$ animals per group. The onset of continuous dietary restriction is indicated by the red arrows. Average age at the onset of tremors is delayed from 9 to

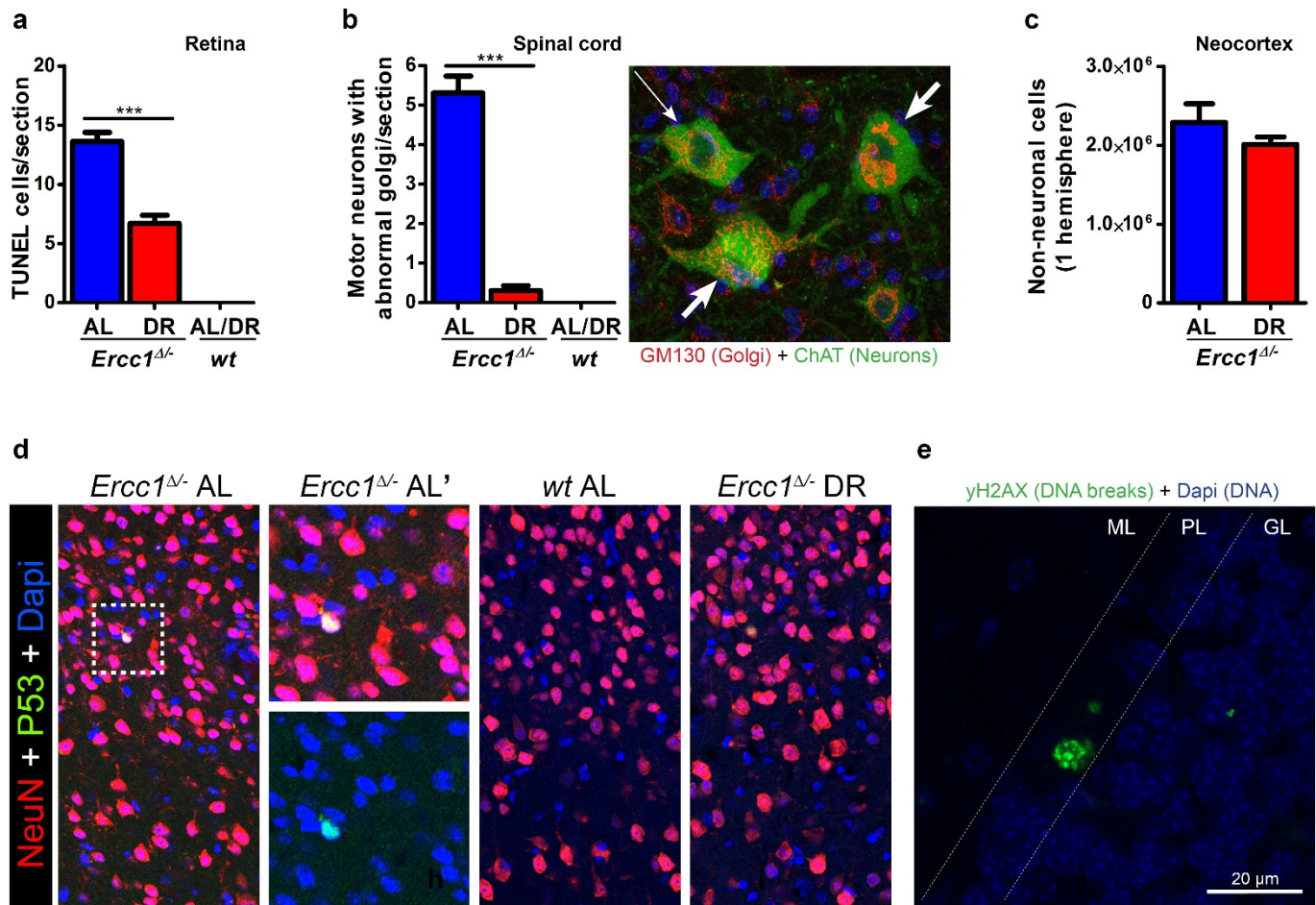
24 weeks, imbalance from 15 to 20 weeks, and paresis from 18 to 26 weeks. Temporary dietary restriction was given between 6 and 12 weeks of age and is indicated in green. This short period of dietary restriction yielded a median delay in onset of tremors of 7 weeks while the median age of onset of both imbalance and paresis was delayed by 3 weeks. P values were calculated against $Xpg^{-/-}$ -*ad libitum* mice using the log-rank test.



Extended Data Figure 5 | See next page for caption.

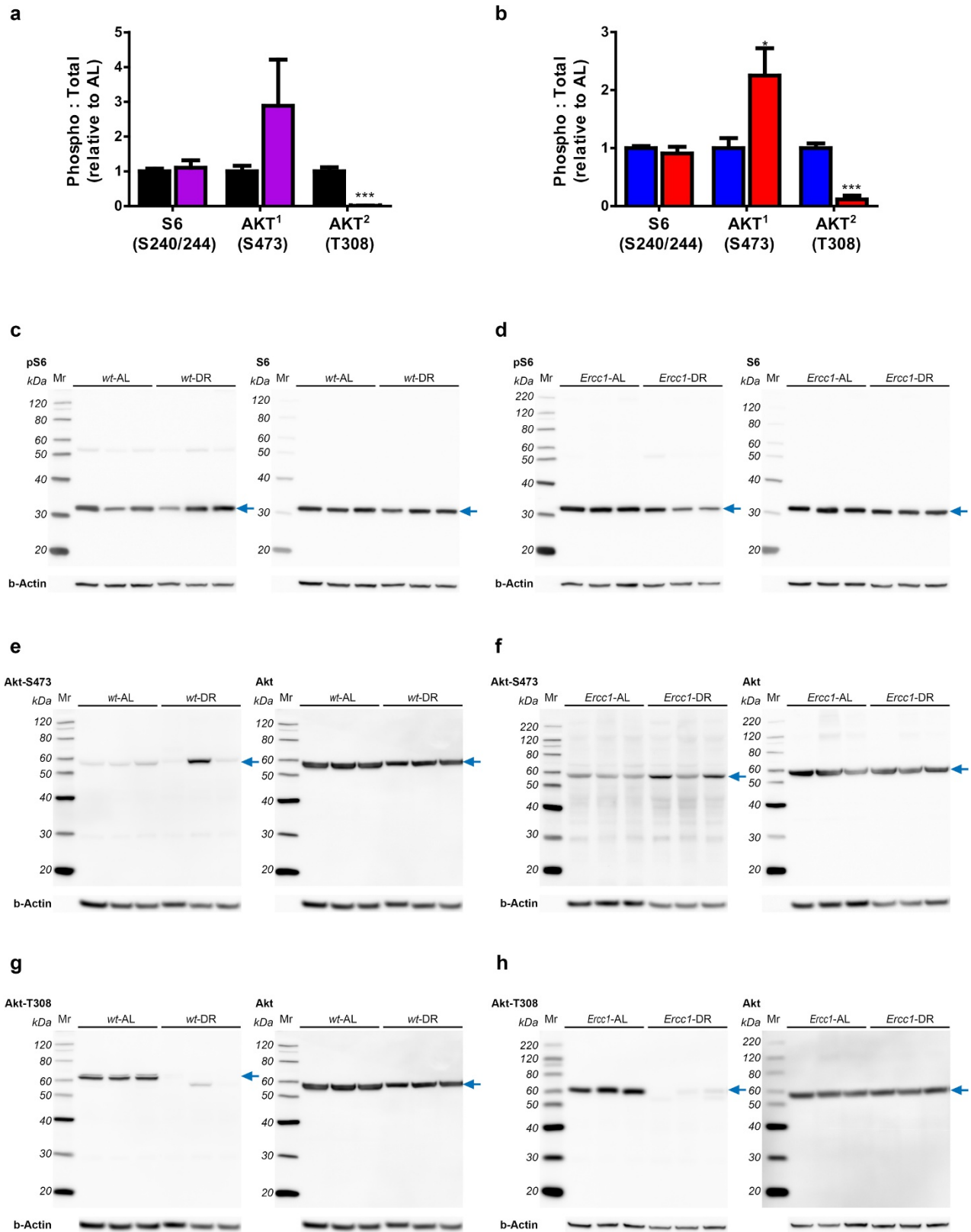
Extended Data Figure 5 | Dietary restriction improves microgliosis and astrocytosis in brain and spinal cord of *Ercc1*^{Δ/-} mice. a–c, Quantification of the relative intensity of consecutive transverse brain and spinal cord sections immunoperoxidase-stained for Mac2 in spinal cord (a) and GFAP in spinal cord (b) and cerebrum (c). $n > 3$ animals per group; bars indicate group medians. **d,** Iba1, Mac2, and GFAP immunofluorescent confocal images showing that reduced astrocytosis (GFAP) in cortex is paralleled by reduced staining for microglia (Iba1). Mac2-immunoreactivity, which outlines a subset of phagocytosing microglia cells, is also reduced in the neocortex of 16-week-old DR^{Ercc1} mice ($n = 4$) when compared to *ad-libitum* mice ($n = 3$). **e–g,** Representative pictures of spinal cord sections of 16-week-old AL^{Ercc1} and DR^{Ercc1} mice immunoperoxidase-stained for Mac2 (e) and GFAP

(f) reflecting reduced microgliosis and astrocytosis, respectively, in the nervous system of diet-restricted mice. Immunoperoxidase-stained spinal cord sections for ATF3 (g) showed that activation of the stress-inducible transcription factor ATF3 (which is induced following genotoxic stress via p53-dependent and -independent pathways) is less pronounced in the nervous system of diet-restricted mice. Sections from two different animals are presented next to each other. Black arrows indicate cells with high nuclear ATF3 staining. **h,** Representative pictures of consecutive transverse brain sections of 16-week-old AL^{Ercc1} and DR^{Ercc1} mice immunoperoxidase-stained for GFAP, showing reduced GFAP staining in the nervous system of diet-restricted mice. Six 40 μm slices are shown per animal, with 360 μm cerebrum thickness between each slice. Mean ± s.e. *** $P < 0.001$.



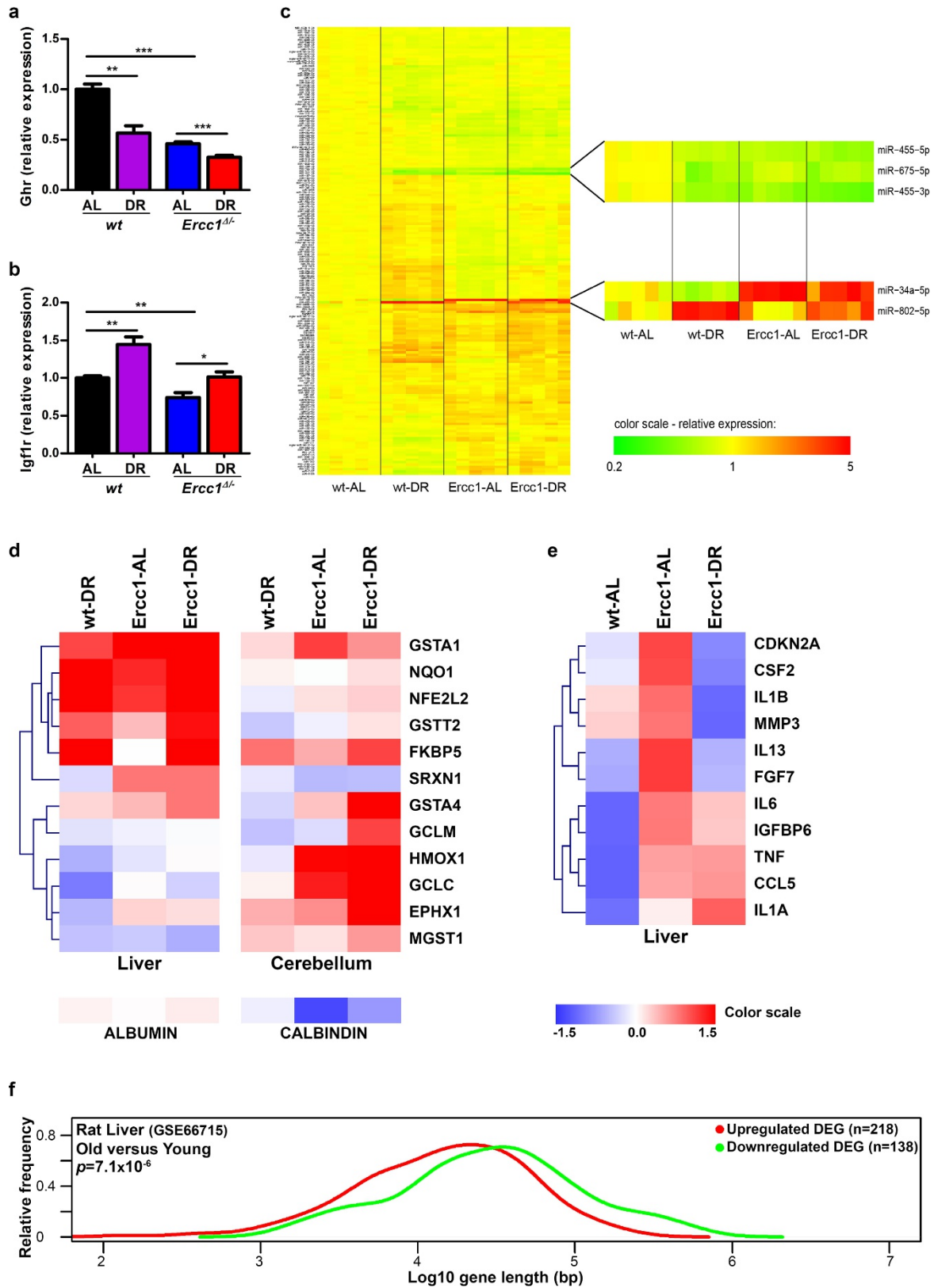
Extended Data Figure 6 | Dietary restriction dramatically preserves neurofunctioning of *Ercc1*^{Δ/Δ} mice. **a**, Quantification of TUNEL-positive cells in the outer nuclear layer of retinal sections of 16-week-old *ad libitum* (blue) or diet-restricted (red) *Ercc1*^{Δ/Δ} mice; $n = 4$ animals per group. **b**, Analysis of the total number of motor neurons with abnormal Golgi apparatus (indicative of impaired cells, see thick arrows in representative image; neuron with normal Golgi is indicated by a thin arrow) in C6 cervical spinal cord sections from 16-week-old diet-restricted and *ad libitum* *Ercc1*^{Δ/Δ} mice. $n = 4$ animals per group. TUNEL-positive cells (**a**) and neurons with abnormal Golgi morphology (**b**) were absent in both *ad libitum*¹⁷ and diet-restricted young wild-type mice. **c**, Quantitative stereological analysis of the total number of non-neuronal cells (DAPI⁺/NeuN⁻; $P = 0.2744$) in the neocortex of transverse brain sections of 16-week-old *ad libitum* and diet-restricted *Ercc1*^{Δ/Δ} mice. $n \geq 3$ animals per group. Mean \pm s.e. *** $P < 0.001$. **d**, Representative images of

neocortex stained for NeuN (neurons), p53 and DAPI (for staining DNA) used for quantitative stereological analysis of the total number of neurons (NeuN⁺) and non-neuronal cells (DAPI⁺/NeuN⁻) in 16-week old *ad libitum*- ($n = 3$) and dietary restriction- ($n = 4$) treated *Ercc1*^{Δ/Δ} mice. Quantification of the number of p53-positive neurons is shown in Fig. 3e. The analysis was performed using the optical dissector probe from StereoInvestigator on a Zeiss LSM700 laser-scanning microscope. **e**, Representative image of cerebellum stained for γH2AX (green, double-stranded DNA breaks) and DAPI (blue, for staining DNA) in 16-week-old *ad libitum* ($n = 3$) and diet-restricted ($n = 4$) *Ercc1*^{Δ/Δ} mice. The Purkinje (PkJ) neurons are present in a single layer (PL, the Purkinje layer) in between the molecular layer (ML) and granular layer (GL)⁴¹. Quantification of the number of γH2AX-positive PkJ-neurons is shown in Fig. 3h. The analysis was performed using a Zeiss LSM700 laser scanning microscope.



Extended Data Figure 7 | Effect of dietary restriction on mTorc1, mTorc2 and Ins/PDK1 signalling using immunoblot analysis of wild-type and *Ercc1*^{Δ/Δ} liver extracts. **a, b,** Quantified relative S6 and Akt phosphorylation by dietary restriction in wild-type (**a**) and *Ercc1*^{Δ/Δ} (**b**) liver extracts. Six animals per group were used at 11 weeks of age. **c–h,** Representative images used to quantify the ratio of S6 and Akt phosphorylation versus total S6 and Akt respectively. Phosphorylation of

Akt at position S473 seems to be increased by dietary restriction in liver homogenates of 11-week-old wild-type (**e**) and *Ercc1*^{Δ/Δ} (**f**) mice, but is suppressed at position T308 (**g, h**). Phosphorylation of S6 at S240 and S244 is unaffected by dietary restriction (**c, d**). For immunoblots, data for three animals per group are shown. For graphs and statistics, six animals per group were used. The blue arrow indicates signals used for quantification. Below each blot, β -actin is presented as a loading control.



Extended Data Figure 8 | See next page for caption.

Extended Data Figure 8 | Molecular analysis of expression changes by diet, DNA damage, or ageing. **a, b**, *Ghr* and *Igf1r* gene expression changes measured by quantitative real-time PCR (qRT-PCR) in liver samples of 11-week old wild-type and *Ercc1*^{Δ/−} mice with restricted diets ($n = 5$). Gene-specific real-time PCR primers are described in Methods. **c**, MicroRNA expression profile comparison of wild-type and *Ercc1*^{Δ/−} mouse liver tissue under *ad libitum* and diet-restricted conditions. Shown are 188 significantly regulated miRNAs (FRD $\leq 5\%$) between groups. Five of the most significantly changed microRNAs are zoomed in. miR-34a, a downstream target of p53 that is involved in cell cycle regulation and apoptosis, is induced by DNA damage^{42,43}. It showed differential expression between liver homogenates of 11-week-old wild-type and *Ercc1*^{Δ/−} mice. It was downregulated by dietary restriction in the liver of wild-type mice (1.62 fold, $P = 0.02$), but strongly upregulated in the liver of AL^{Ercc1} mice compared to AL^{WT} mice (4.7-fold, $P = 0.0001$) and seems suppressed in DR^{Ercc1} expression profiles. These changes were confirmed by qPCR (data not shown). **d**, Heat map of key antioxidant defence genes in liver and brain of wild-type and *Ercc1*^{Δ/−} mice. Fold changes were calculated for DR^{WT}, AL^{Ercc1}, and DR^{Ercc1} mice against AL^{WT} mice, using microarray expression profiles of liver tissue at 11 weeks of age ($n = 5$) or qRT-PCR for cerebellum tissue at 16 weeks of age ($n = 4$). Dietary restriction induced an antioxidant response in liver, which is less pronounced in brain specimens, consistent with earlier findings⁴⁴. This is likely to be due to the high endogenous antioxidant defence levels in the nervous system. The difference in antioxidant response between liver and brain by genotype conforms to previous results⁶. Interestingly, the Purkinje neuron marker calbindin is clearly reduced in cerebella of AL^{Ercc1} mice but is less reduced in DR^{Ercc1} mice, confirming the strong reduction in DNA-damage-induced Purkinje cell loss induced by dietary restriction. Blue, decreased expression; red, increased expression. Hierarchical clustering on liver and cerebellum genes was performed using a Pearson correlation. **e**, Dietary restriction reduces the p16-RB branch of senescence and the senescence-associated secretory phenotype (SASP)

as assessed by next-generation sequencing expression analysis of the liver RNA of *Ercc1*^{Δ/−} mice. To assess the p16-RB branch of the senescence phenotype⁴⁵, we followed a next-generation sequencing approach as previously described³⁶ using 16-week-old liver tissue from AL^{WT}, DR^{WT}, AL^{Ercc1} and DR^{Ercc1} mice ($n = 1$). By sequencing $>150\text{M}$ sequence reads per sample, we detected the *p16-ink4a* (*Cdkn2a*) transcript at sufficient levels. *p16-ink4a* (*Cdkn2a*) is considered a key marker for cellular senescence, but is difficult to quantitatively analyse using other methods owing to the high ratio of normal cells to senescent cells. Data sets were normalized by calculating reads per kilobase million (RPKM). Subsequently, z -scores were calculated and plotted in a heat map. Red, increased expression; blue, decreased expression. In AL^{Ercc1} liver RNA, *p16-ink4a* (*Cdkn2a*) is upregulated compared to levels in AL^{WT} animals, but downregulated after dietary restriction. This indicates that *Ercc1*^{Δ/−} mice have increased cellular senescence that is reduced upon dietary restriction. Second, we monitored the transcriptionally induced SASP as described previously⁴⁶. Many, if not all, SASP factors are not exclusively specific for cellular senescence. To reduce the probability that observed SASP factor expression changes are contributed to by other cells, we selected only those SASP factors that have an absolute expression (RPKM) in the same range as *p16-ink4a* in across these data sets, since these are most likely to be the result of cellular senescence. The figure shows that most SASP factors such as *IL-6*, the most prominent SASP cytokine are downregulated after dietary restriction. This supports the idea that cellular senescence and associated SASP are increased in AL^{Ercc1} liver and are reduced by dietary restriction. Hierarchical clustering was performed using a Pearson correlation. **f**, Suppression of long genes in normal ageing of rat liver. A relative-frequency plot of the gene length of DEGs in liver tissue from 24-month old rat versus that seen in 6-month old rat. Upregulated genes, red; downregulated genes, green. The DEGs from rat liver were selected using a fold-change cut-off of 1.5 and an FDR < 0.05 . The data set is publicly available in the NCBI Gene Expression Omnibus under accession number GSE66715.

Extended Data Table 1 | Discordant DEG in dietary restriction response for wild-type and *Ercc1*^{Δ/-} mice

ProbeID	Gene Symbol	logFC wt-DR vs wt-AL	P.Val Wt-DR vs wt-AL	logFC Ercc1-DR vs Ercc1-AL	P.Val Ercc1-DR vs Ercc1-AL
1438583_PM_at	Ern1	0.77	0.003	-0.74	0.010
1438997_PM_at	Ern1	0.69	0.005	-0.70	0.010
1429295_PM_s_at	Trip13	-0.72	0.005	0.77	0.007
1441098_PM_at	Pnlc1	-0.66	0.030	1.10	0.002

DEG in common in dietary restriction response in liver of wild-type and *Ercc1*^{Δ/-} mice but with discordant direction of change.

Extended Data Table 2 | Average gene length of up- and downregulated genes of wild-type and *Ercc1*^{Δ/-} liver expression profiles under *ad libitum* and diet-restricted conditions

Comparison	Length (bp) means	wilcox.test
Wt-DR Up vs. <i>Ercc1</i> -AL Up	66,364 vs. 40,021	< 2.2e-16
Wt-DR Down vs. <i>Ercc1</i> -AL Down	62,352 vs. 212,957	< 2.2e-16
Wt-DR Up vs. <i>Ercc1</i> -DR Up	66,364 vs. 41,284	< 2.2E-16
Wt-DR Down vs. <i>Ercc1</i> -DR Down	62,352 vs. 141,391	3.24E-14
<i>Ercc1</i> -AL Up vs. <i>Ercc1</i> -DR Up	40,021 vs. 41,284	0.001
<i>Ercc1</i> -AL Down vs. <i>Ercc1</i> -DR Down	212,957 vs. 141,391	0.0002

Comparisons of the mean gene size distributions of DEGs (up- and downregulated) among DR^{WT} versus AL^{WT}, AL^{*Ercc1*} versus AL^{WT} and DR^{*Ercc1*} versus AL^{WT} in mouse liver tissue. wt-DR Up, shows the number of DEGs that are upregulated in DR^{WT} compared with AL^{WT} ($n = 1,106$); wt-DR Down shows the number of DEGs that are downregulated in DR^{WT} compared with AL^{WT} ($n = 1,046$); *Ercc1*-AL Up shows the DEGs that are upregulated in AL^{*Ercc1*} compared with AL^{WT} ($n = 595$); *Ercc1*-AL Down shows the DEGs that are downregulated in AL^{*Ercc1*} compared with AL^{WT} ($n = 363$); *Ercc1*-DR UP shows the number of DEGs that are upregulated in DR^{*Ercc1*} compared with AL^{WT} ($n = 1,384$); *Ercc1*-DR Down shows the number of DEGs that are downregulated in DR^{*Ercc1*} compared with AL^{WT} ($n = 768$). Because the distributions of the gene lengths do not have a normal distribution the means should be taken as a reference value.